

1 **EcoTWIN 1.0: A Fully Distributed Tracer-Aided Ecohydrological Model Tracking Water,** 2 **Isotopes, and Nutrients**

3 Songjun Wu¹, Doerthe Tetzlaff^{1,2}, Yi Zheng³, Chris Soulsby⁴

4 1 Department of Ecohydrology and Biogeochemistry, Leibniz Institute of Freshwater Ecology and
5 Inland Fisheries, Berlin, Germany

6 2 Geography Institute and IRI THESys, Humboldt University of Berlin, Berlin, Germany

7 3 School of Environmental Science and Engineering, Southern University of Science and Technology,
8 Shenzhen, China

9 4 Northern Rivers Institute, School of Geosciences, University of Aberdeen, UK

10 Corresponding author: Songjun Wu (songjun.wu@igb-berlin.de)

11

12 **Abstract**

13 The value of stable water isotopes in constraining process representation in hydrological models is
14 well acknowledged with numerous tracer-aided hydrological models developed in recent years, yet
15 few have leveraged these benefits for more robust water quality modelling. Therefore, we introduce
16 EcoTWIN, a fully distributed tracer-aided ecohydrological model that simultaneously **tracks water,**
17 **isotope,** and **nutrient** fluxes. A thorough model test was conducted by calibrating EcoTWIN against
18 discharge, in-stream isotopes, and NO₃-N concentrations (1980-2024) in 17 large-scale (10³ - 10⁵ km²)
19 European catchments spanning a wide range of geographic and climatic gradients. Furthermore, three
20 reanalysis products (ERA5 snow depth, MODIS evapotranspiration, and GRACE surface water anomaly)
21 were employed to further validate the capacity of EcoTWIN to reproduce associated but uncalibrated
22 internal water fluxes. Results showed good model performance of both calibrated in-stream targets
23 and uncalibrated internal fluxes in most catchments. Therefore, we conclude that EcoTWIN is a flexible,
24 transferable modelling tool for prediction and process inference in terrestrial ecosystems ranging from
25 boreal to subtropic climates. Constrained by tracer simulations, the model not only captures the
26 celerity, but also the velocity of hydrological fluxes, thus providing spatio-temporally-explicit
27 estimations of water ages and travel times. Such information provides opportunities to bridge
28 catchment hydrology and water quality by linking travel times with biogeochemical processing
29 **timeskinetics**. We demonstrate this with a proof of concept using Damköhler Number in nitrogen
30 modelling.

31

32 **1 Introduction**

33 The development of ecohydrological models has been accelerating in the recent decades towards
34 frameworks that are more spatially distributed (instead of lumped or semi-distributed) and complex
35 (integrating more ecohydrological processes) (Pechlivanidis et al., 2011; Wellen et al., 2015). A few
36 examples include SWAT (Arnold et al., 2012), HYPE (Lindström et al., 2010), and mHM-Nitrate (Yang
37 et al., 2018), which have been widely applied worldwide. As process-based models, they are used not

38 only as prediction tools for specific variables, but also as learning tools for model inference, i.e., to
39 track the internal states/fluxes from available observations (Wang et al., 2024). This, however, poses
40 challenges due to the considerable uncertainties in model inference.

41 Inference of internal processes is naturally uncertain due to the lack of direct observations, though
42 such uncertainty can be constrained to some extent by rigorous split-sample calibration and validation.
43 The reason we use “somehow” here is based on the fact that most models are calibrated to a minimal
44 number of variables, and 81% of calibrations used data from a single gauge (mostly at a catchment
45 outlet) as reviewed in Wellen et al., (2015). Additionally, from a technical perspective, “equifinality”
46 further adds to the inference uncertainty due to the potential misinformation in data (uncertainty in
47 model forcing and observations) and model structure (the use of simplified, abstract mathematics to
48 simulate real world processes) (Beven, 2006). This can result in inaccurate process representations
49 yielding deceptively good results through error compensation, thus leading to overconfidence in a
50 model's ability to reproduce within-basin dynamics (Wen et al., 2024; Wu et al., 2025a). As
51 acknowledged by the hydrological community, models calibrated solely against discharge at the
52 catchment outlet reflect only the celerity of hydrological systems (pressure wave propagation), yet
53 constituent transport in water quality modelling relies on the velocity (mass flux of the water)
54 (McDonnell & Beven, 2014). Failure to reconcile these differences can lead to questionable process
55 inferences from many ecohydrological and water quality models.

56 One way to strengthen model inference is to include auxiliary data for calibration (Efstratiadis &
57 Koutsoyiannis, 2010). However, there is a paradox in multi-criteria calibration, as on the one hand,
58 more auxiliary data will feed unique information to the calibration process, thus effectively
59 constraining the model behaviour from an ecohydrological perspective; yet on the other hand, it
60 increases the dimensionality of calibration thus resulting in degraded performance or failure of
61 calibration from a technical perspective. The “curse” of dimensionality in ecohydrological modelling is
62 universal for all the commonly used algorithms under both Bayesian and Pareto theories as
63 demonstrated in Wu et al., (2025c). Therefore, modellers should expect the selected auxiliary data to
64 contain as much information as possible (Nearing et al., 2020). For distributed modelling, the auxiliary
65 data should reflect the cumulative contribution of all upstream reaches/regions, rather than variables
66 that are highly dependent on local condition/processes (e.g. point-scale soil moisture and
67 evapotranspiration measurements etc.).

68 Stable water isotopes, in this context, have powerful potential in cumulative flux tracking. As
69 conservative tracers, ^2H and ^{18}O are independent of biogeochemical reactions and naturally integrate
70 landscape heterogeneity, thus providing effective constraints on spatially distributed (dis)connections
71 of hydrological flow paths as well as velocity of the hydrological systems which reflect flux-storage
72 interactions (Jung et al., 2025; Tetzlaff et al., 2015). The value of tracers has long been recognised by
73 hydrologists (Hooper et al., 1988), with many tracer-aided hydrological models developed and evolved
74 in recent years from lumped (Birkel et al., 2011; Godsey et al., 2010), to semi-distributed (van
75 Huijgevoort et al., 2016; Nan et al., 2021), and distributed structure (Kuppel et al., 2018; Remondi et
76 al., 2018). However, few attempts have been made to integrate a tracer-aided hydrological structure

77 into water quality modelling (Birkel & Soulsby, 2015; Jung et al., 2025), despite the need being evident
78 for nearly four decades (Neal et al., 1988). Moreover, existing pioneering models are mostly
79 conceptualised/lumped (Benettin et al., 2015; Dick et al., 2015) and/or loosely coupled via external
80 tracer/water quality modules (Pesántez et al., 2023; Yang et al., 2024; Zhang et al., 2020). The external
81 coupling of model chains transfer necessary internal states and fluxes between sub-models (e.g.
82 hydrological fluxes for constituent mixing in water quality or isotopic modules) via online in-memory
83 coupling (instead of offline on-disk coupling), thus significantly increasing the resources consumption
84 in input/output operations. Such model chains, though providing useful scientific insights, can become
85 problematic for large-scale applications owing to the exponential growth in computational and
86 storage requirements. Therefore, there remains a need to develop a fully distributed, computationally
87 efficient ecohydrological model that combines hydrological, isotopic, and water quality simulations.

88 This research gap motivated the development of EcoTWIN, the model that we present in this paper.
89 To our knowledge, the model is one of the first distributed tracer-aided **ecohydrological** models that
90 **tracks water, isotopic, and nutrient** fluxes simultaneously in a C++-based framework. For a thorough
91 testing of EcoTWIN, 17 large European catchments were selected for calibration against discharge, in-
92 stream isotopes, and NO₃-N concentrations. These catchments span over a wide range of geographic
93 (Alpine to lowland plain) and climatic (from snow-dominated to Mediterranean) gradients. In addition,
94 the robustness of modelled inference on uncalibrated internal fluxes were also compared with three
95 remote sensing products (snow depth, evapotranspiration, and water storage). Given the overall good
96 integrated performance in most catchments, EcoTWIN is presented as an ecohydrological modelling
97 framework applicable for terrestrial ecosystems ranging from boreal to temperate and subtropical
98 climates across a wide range of geographical environments. The subsequent sections are organised as
99 follows: Section 2 and 3 introduce the model structure of EcoTWIN and details in calibration and
100 validation; the model performance is shown in Section 4; in Section 5 we show the advantages of a
101 tracer-aided ecohydrological framework with an example of how water ages bridge catchment
102 hydrology and water quality models; finally, the current limitations and planned future development
103 of EcoTWIN are also discussed.

104

105 **2 Model description**

106 EcoTWIN is fully distributed ecohydrological model implemented in C++. The model consists of
107 hydrological, isotopic, and nitrogen modules, which simulate major ecohydrological states and fluxes
108 from canopy to groundwater (Figure 1). Aided by tracer simulations, the model is additionally able to
109 track the water movement vertically and laterally via the calculation of water ages and travel times.
110 For detailed information of model parameters please refer to Table S1.

111

112 2.1 Hydrological module

113 EcoTWIN follows a typical multi-layer, top-down, bucket-type approach that resolves the water
114 balance sequentially for the vegetation canopy, three soil layers, unsaturated zone, and groundwater.
115 As the foundation of solute transport, the hydrological module employs a selective disassembly
116 structure with multiple alternative conceptualisations possible for specific important hydrological
117 processes. The configuration can be specified *a priori* based on the goal of modelling and prior
118 knowledge of the studied catchment(s).

119 2.1.1 Soil properties

120 Before iterative simulations, soil characteristics are estimated using appropriate pedotransfer
121 functions. Three different alternatives are provided, each of which requires different levels of inputs
122 but all were found to provide robust estimation of soil porosity (θ_s), field capacity (θ_{fc}), wilting point
123 (θ_{wp}), and hydraulic conductivity (Ks). All the soil properties are required for each soil layer/depth.
124 This can be achieved via three alternative options: (i) assigning identical properties across the whole
125 soil column, (ii) calculating separately for each depth based on depth-dependent inputs, or (iii)
126 extrapolating deeper profile characteristics from the top soil properties based on a depth-dependent
127 equation in Maneta & Silverman, (2013).

128 The distribution of soil types and land use is assigned from raster file in EcoTWIN. This can be specified
129 as a static boundary condition; alternatively, the distributions can also be updated dynamically via a
130 user-specified interval to reflect any temporal changes due to land management.

131

132 2.1.2 Vertical fluxes

133 The vertical fluxes are resolved for storages in the canopy, soil layers, unsaturated zone, and
134 groundwater. The mass balance of canopy storage (ΔC) follows:

$$\Delta C = P - I - Th \quad (1)$$

135 where P , I , Th are precipitation, interception, and throughfall, respectively. The throughfall is
136 calculated as the exceedance of current canopy storage from the maximum storage calculated by Leaf
137 Area index LAI and a correlation parameter α .

$$C_{max} = \alpha * LAI \quad (2-1)$$

138 Alternatively, the maximum canopy storage can be estimated with explicit consideration of
139 precipitation intensity (Landgraf et al., 2023):

$$C_{max} = \alpha * LAI * \left(1 - \frac{1}{1 + SCF * P / (\alpha * LAI)}\right) \quad (2-2)$$

140 where SCF is the vegetation cover fraction calculated by LAI and an extinction coefficient (rE)
141 adopted from HYDRUS-1D (Šimůnek et al., 2013):

$$SFC = 1 - \exp(rE * LAI) \quad (3)$$

142 Then throughfall is calculated as the exceedance of canopy storage from the maximum:

$$Th = (P + C) - C_{max} \text{ if } (P + C) > C_{max} \text{ else } 0 \quad (4)$$

143 After reaching land surface, throughfall becomes ponding water (S_{Pond}) or snow (S_{Snow}) depending
144 on a temperature threshold for separation ($Thre_{SN}$). Snow will melt and recharge the ponding water
145 in warm conditions (air temperature Ta exceed $Thre_{SN}$) following a degree-day model.

$$melt = S_{Snow} * \min(dd_{min} + dd_{inc} * Th * (Ta - Thre_{SN}), dd_{max}) \quad (5)$$

146 Where dd_{min} and dd_{max} are the minimum and maximum of degree day factor, while dd_{inc} denotes
147 the rate of increase in the degree-day factor per degree Celsius rise in temperature.

148 The available ponding water infiltrates into the top soil layer using Green-Ampt model (Kale & Sahoo,
149 2011; Maneta & Silverman, 2013), with infiltration capacity first calculated as a function of average
150 soil moisture over the hydrologically active depth:

$$I_f = K_S * \left(1 + \frac{\psi * \theta_s * (1 - (\theta_1 - \theta_{wt}) / (\theta_s - \theta_{wt}))}{\theta_1 * d_1}\right) \quad (6)$$

151 Where θ_1 , θ_s , θ_{wt} , and d_1 are the moisture content, porosity, wilting point, and depth in top soil layer;
152 ψ is a parameter representing soil air entry pressure in m. Then potential infiltration (F_p) is determined
153 from the lesser between the available ponding water (S_{pd}) and potential infiltration rate integrated
154 over time before ponding occurs ($I_f * t_p$).

155 The actual infiltration (F) is solved iteratively using the Newton–Raphson scheme:

$$F = \Delta\theta * d_1 = F_p + K_S * w_{K_S} * (\Delta t - t_p) - \psi \Delta\theta * \ln\left(\frac{\psi \Delta\theta + \Delta\theta d_1}{\psi \Delta\theta + F_p}\right) \quad (7)$$

156 where w_{K_S} is anisotropy ratio of vertical to horizontal K_S .

157 The soil storage in each layer is conceptualised as two water pools – a gravitational, free-flowing pool
158 and a capillary, soil-bound pool. The two pools are separated based on field capacity (Maneta &
159 Silverman, 2013), and percolation happens when soil storage exceeds the threshold. Three alternative
160 schemes are included in EcoTWIN.

161 In the first scheme, all water in excess of field capacity percolates to deeper layer:

$$Pc_i = (\theta_i - \theta_{fc}) * d_i \quad (8-1)$$

162 where Pc_i , θ_i and d_i depict the percolation, moisture content and depth from/in i th soil layer in m.

163 The second scheme additionally considers the hydraulic conductivity (K_S) following the
164 conceptualisation in SWAT (Arnold et al., 2012):

$$Pc_i = (\theta_i - \theta_{fc,i}) * d_i * \left(1 - \exp\left(\frac{-\Delta t * K_S}{\theta_{s,i} - \theta_{fc,i}}\right)\right) \quad (8-2)$$

165 The third scheme relates percolation to the extent of soil saturation with an exponential parameter β
 166 (Kumar et al., 2013; Samaniego et al., 2010):

$$Pc_i = (\theta_i - \theta_{fc,i}) * d_i * (1 - \exp(\beta * \log(\theta_i/\theta_{s,i}))) \quad (8-3)$$

167 For evapotranspiration, soil evaporation and transpiration are estimated separately. The separation
 168 of PET is realised by surface cover fraction introduced above:

$$PT = PET * SCF; \quad PE = PET - PT \quad (9)$$

169 Soil evaporation is simulated in the top soil layer based on the soil saturation:

$$Evap_s = PE * \min\left(\frac{\theta_1}{\theta_{fc,1}}, 1\right) \quad (10)$$

170 Transpiration is simulated in all soil layers based on the fractions ($f_{root,i}$) of root density ($D_{root,i}$) in
 171 each layer partitioned by soil depth and a parameter (γ_{root}):

$$Tr_i = PT * f_{root,i} * \frac{\theta_1 - \theta_{wp,1}}{\theta_{fc,1} - \theta_{wp,1}} \quad (11)$$

$$f_{root,i} = D_{root,i} / \sum_{j=1}^m D_{root,j} \quad (12)$$

$$D_{root,i} = \left(1 - \gamma_{root}^{\left(\sum_{j=1}^m d_j\right)}\right) - \left(1 - \gamma_{root}^{\left(\sum_{j=1}^i d_j\right)}\right) \quad (13)$$

172 Channel evaporation is also estimated using Penman equation, which relies on net radiation, wind
 173 speed, air pressure, and air temperature as inputs.

174 The last soil layer percolates to an unsaturated storage in unsaturated zone (S_{unsat}). The
 175 compartment stores the excess water from soil and percolates either downward to groundwater
 176 storage (S_{GW}) or laterally downstream. The percolation to groundwater Pc_{GW} is determined by a
 177 weighting parameter p_{GW} as a proportion of unsaturated storage:

$$Pc_{GW} = S_{unsat} * p_{GW} \quad (14)$$

178 Additionally, irrigation is conceptualised in EcoTWIN, which is realised via the water extraction from
 179 river or groundwater. The source is determined by the geographic location: for a grid cell with channel
 180 network, water is extracted directly from river, and local groundwater is used as irrigation source for
 181 non-channel grids. The amount of extraction is estimated from a predefined coefficient for crop water
 182 demands (w_{irr}) from which the deficit is calculated for each of the m soil layers.

$$deficit = \sum_{i=1}^m (\theta_{fc,i} - \theta_{wp,i}) * w_{irr} * d_i \quad (15)$$

183 Note that the irrigation can switch to groundwater extraction if river storage cannot fill the deficit.

184

185 **2.1.3 Lateral fluxes**

186 In EcoTWIN, grid cells are connected laterally at three levels - surface, unsaturated zone, and
 187 groundwater. Note that some models omit the unsaturated storage and directly calculate excess
 188 water to drain based on the saturation extent of the bottom soil layer (e.g., ECH₂O-iso, Kuppel et al.,
 189 2018). EcoTWIN did not follow this conceptualisation because in reality, the lateral drainage is focused
 190 in the saturated zone, and thus the bottom of the soil layer instead of the whole soil profile. The
 191 drainage of an entire soil layer thus brings considerable uncertainty to the velocity of lateral transport
 192 when the lower boundary of the soil is a parameter to tune in calibration. For instance, a large soil
 193 depth will dramatically reduce the velocity of interflow drainage and slow down the mixing of
 194 constituents, though this might still perfectly reproduce the celerity (hydrograph) for purely
 195 hydrological modelling. Our conceptualisation (an independent unsaturated compartment) aligns
 196 with most hydrological models (Arnold et al., 2012; Yang et al., 2018) and fits the recent analysis
 197 supporting the dominant role of lateral drainage over vertical transports globally (Mcmillan et al.,
 198 2025).

199 By the end of each timestep, ponding water receives upstream inputs and contributes to channel
 200 storage if the grid is connected to the channel network, while non-channel grid has $Ovf_C = 0$:

$$Ovf_C = (Ovf_{T,in} + S_{pond}) * p_{Ovf} * dx_C/dx_T \quad (16)$$

201 dx_C and dx_T are the channel length and size of terrestrial grid cell; p_{Ovf} is a weighting parameter for
 202 channel recharge. Then the remaining ponding water routes to downslope terrestrial grid following
 203 the topographic gradient. In none-channel grid cells, all available ponding storage routes lateral
 204 downstream ($Ovf_C = 0$):

$$Ovf_{T,out} = (Ovf_{T,in} + S_{pond}) - Ovf_C \quad (17)$$

205 Similarly, unsaturated storage contributes first to channel storage in grid cells within channel network,
 206 while non-channel grid cells have $Inf_C = 0$:

$$Inf_C = (Inf_{T,in} + S_{vadose}) * K_{vadose} * \left(1 - e^{-1 * exp_{Inf} * (Inf_{T,in} + S_{vadose})}\right) * p_{Inf} \quad (18)$$

207 where K_{vadose} is the effective conductivity of lateral transport in the unsaturated zone; while exp_{Inf}
 208 is an exponential parameter determining the strength of positive correlation between recharge and
 209 current unsaturated storage. Then the remaining unsaturated storage is partially routed to downslope
 210 grid cell following a linear approximation of Kinematic wave equation, which assumes gravitational
 211 flux per unit width $Inf_{T,out}$ is proportional to the subsurface hydraulic conductivity (K_{vadose}) and
 212 bedrock slope ($slope$ approximated from the surface slope):

$$Inf_{T,out} = (Inf_{T,in} + S_{unsat} - Inf_C) * \left(1 + \alpha * \frac{dt}{dx}\right) * \alpha * \frac{dt}{dx} \quad (19)$$

$$\text{where } \alpha = K_{unsat} * \sin(slope)$$

213 Groundwater routing is similar to that of interflow, with channel recharge followed by terrestrial
 214 transport. Note that the terrestrial groundwater flow does not consider the bedrock slope as

215 groundwater storage is generally much large than unsaturated storage, and thus independent from
 216 topographic gradients:

$$GWf_C = (GWf_{T,in} + S_{GW}) * K_{GW} * \left(1 - e^{-1 * exp_{GWf} * (GWf_{T,in} + S_{GW})}\right) * p_{GWf} \quad (20)$$

$$GWf_{T,out} = (GWf_{T,in} + S_{GW} - GWf_C) * \left(1 + \alpha * \frac{dt}{dx}\right) * \alpha * \frac{dt}{dx} \quad (21)$$

where $\alpha = K_{vadose}$

217 The channel routing is realised using Kinematic wave equation based on a scaled channel roughness
 218 parameter (Maneta & Silverman, 2013).

219

220 **2.2 Isotopic module**

221 The isotopic module in EcoTWIN tracks the composition of stable water isotopes in all water storage
 222 compartments following hydrological mixing and fractionation. The module also provides estimation
 223 of water age and travel time conceptualised as the time since water molecules enter the catchment
 224 as precipitation, and the time water molecules need to travel through the specific storage.

225 **2.2.1 Mixing**

226 The mixing and transport of isotopes (^2H and ^{18}O , both noted as C) are governed by the velocity of
 227 hydrological fluxes with a complete mixing strategy for most water storages:

$$\frac{d(V * C)}{dt} = \sum_{k=1}^{N_{in}} q_{in,k} * C_{in,k} - \sum_{k=1}^{N_{out}} q_{out,k} * C \quad (22)$$

228 Where V and C are the volume and composition/concentration of the storage, while N_{in} and N_{out}
 229 denote the number of influx and outflux. Such strategy is built on two assumptions: (i) constitutes (i.e.,
 230 isotopes) are fully mixing within each timestep; (ii) the composition/concentration in outflow equals
 231 to that in storage. Additional mixing between ponding and upper soil water storage is allowed (with
 232 proportion determined by a parameter $SrfMixing$), as nutrients in top soils can be flushed out in
 233 large hydrological events (Seybold et al., 2022).

234 The full-mixing assumptions have been widely used and shown to be reasonable for storages with
 235 relatively small volumes in many mixing/water quality models (Arnold et al., 2012; Yang et al., 2018).
 236 However, some studies show that a complete mixing strategy can be problematic for large storages
 237 such as groundwater as they are generally poorly constrained (e.g. Soulsby et al., 2015). Therefore,
 238 the mass conservation equation used in the INCA-N model and mHM-Nitrate is employed to calculate
 239 the mixing of groundwater storages with influxes (i.e., percolation from unsaturated storage and
 240 lateral groundwater inflow).

$$\frac{dC}{dt} = \frac{1}{V + V_r} * \left(\sum_{k=1}^{N_{in}} q_{in,k} * C_{in,k} - \sum_{k=1}^{N_{out}} q_{out,k} * C \right) \quad (23)$$

241 where V_r is the retention storage. The equation is solved by the fourth order Runge-Kutta technique.

242

243 **2.2.2 Fractionation**

244 As conservative tracers, the composition of isotopes in water storages/fluxes is only changed by
245 kinetic fractionation apart from hydrological mixing. The process is accompanied by evaporation,
246 resulting in the preferential loss of lighter isotopes (^1H and ^{16}O) to the vapor phase and a
247 corresponding enrichment of heavier isotopes (^{18}O and ^2H) in the residual water. In EcoTWIN, the
248 fractionation is simulated along with evaporation of top soil water and river storage based on the
249 Craig-Gordon model (Craig et al., 1964; Kuppel et al., 2018), while transpiration is assumed to be a
250 non-fractionating process (Dawson & Ehleringer, 1991; Kuppel et al., 2018).

$$C = C^* - (C^* - C) * \left(\frac{S - Evap}{S} \right)^m \quad (24)$$

251 where C^* and m are the limiting isotopic composition (in ‰) and the dimensionless enrichment slope
252 that are estimated via the following equations in (Good et al., 2014):

$$C^* = \frac{h_a C_a + h_s \varepsilon^+ + \varepsilon^k}{h_s - h_a + \varepsilon^k / 1000} \quad (25)$$

$$m = \frac{h_a - (h_s \varepsilon^+ + \varepsilon^k) / 1000}{h_s - h_a + \varepsilon^k / 1000} \quad (26)$$

253 where h_a is the relative humidity above the soil surface normalised from atmospheric relative
254 humidity (h), air temperature (T_a), and soil temperature (T_s estimated from Amato & Giménez, 2024).
255 C_a is the isotopic composition of ambient air moisture estimated from precipitation composition:

$$C_a = (C_{rain} - \varepsilon^+) / \alpha^+ \quad (27)$$

256 where ε^+ is the equilibrium fractionation factor (Skrzypek et al., 2015); α^+ is a temperature factor
257 estimated from T_a .

$$\varepsilon^+ = (1 - 1/\alpha^+) * 1000 \quad (28)$$

258 The factor of diffusion-controlled kinetic isotopic separation ε^k is calculated based on the relative
259 humidity of soil surface (h_a) and soil pore (h_s).

$$\varepsilon^k = (h_s - h_a) * \left(1 - \frac{D_i}{D} \right) * n \quad (29)$$

260 Where D_i and D denote the diffusivities of water vapor molecules containing heavier isotope and the
261 lighter isotope, respectively. The ratio can be acquired in Horita et al., (2008) for ^2H (0.9877) and ^{18}O
262 (0.9859). n is an advection term ranging between 0.5 (in saturated soils) and 1 (in dry soils). The factor
263 is included in calibration for the fractionation of top soil evaporation yet fixed as 0.5 for that of channel
264 evaporation.

265

266 **2.2.3 Water age and travel time**

267 EcoTWIN can track the age of water i.e., the time since water enters the catchment as precipitation,
268 in each storage. In age tracking, precipitation is defined as new water with age of zero. At the end of
269 each time step, water ages of all storages are advanced based on the temporal resolution (for instance
270 one day if the model is set up for daily timesteps). Note that in some circumstances, the modellers
271 might need to disable the age evolution of specific storage(s) (e.g., groundwater storage) as the
272 storage can be too large to achieve steady states in model spin-up. Similar to isotopes, water ages are
273 only controlled by hydrological transport with the same mixing strategy (i.e., complete mixing except
274 for groundwater).

275 The water ages in EcoTWIN are the mean values averaged from all water molecules in the storage,
276 which might be dominated by the inflow of very old water that obscure the age distribution of the
277 young water (e.g., the groundwater input to top soils due to the groundwater extraction for irrigation).
278 Therefore, EcoTWIN additionally provides the estimation of travel time - the time of water molecule
279 travelling through each storage. The simulation is similar to that of water ages. The only difference is
280 that the transition of water between storages (e.g., percolation into deeper soil layers) resets the travel
281 time to zero. Accordingly, all the water enters a new storage becomes new water instead of just
282 precipitation in water age tracking.

283

284 **2.3 Nitrogen module**

285 The nitrogen module describes the mass balance of nitrogen, particularly nitrate as the main form of
286 dissolved nitrogen, which is dominated by the interaction of hydrological transport and
287 biogeochemical transformations.

288 For each timestep, the nitrate concentration is simulated in each storage following three processes –
289 hydrological transport/mixing, nitrogen inputs, and biogeochemical transformations. Fully integrated
290 with hydrological module, nitrate transport also aligns with hydrological fluxes following the same
291 mixing strategy as in the isotopic simulation. For nitrogen sources, EcoTWIN considers the inputs from
292 fertiliser, manure, and plant residues, whose annual inputs can be specified via configuration. Notably,
293 fertilization can be parameterised via spatial raster inputs if corresponding dataset is available. The
294 timing and extent of nitrogen addition of all sources are determined following the implementation in
295 HYPE (Lindström et al., 2010), which distributes the annual sum across a specified period (e.g., the
296 period between planting and harvest for crops). Additionally, wet deposition is conceptualised as the
297 atmospheric nitrogen source, whose concentration can be specified via spatial raster and simply as a
298 constant value.

299 The biogeochemical transformations are mainly modified from the mHM-Nitrate model (Yang et al.,
300 2018), and the HYPE model (Lindström et al., 2010), which are conceptualised for the soil profile and
301 channel network. In the soil profile, three nitrogen pools are conceptualised for each soil layer,
302 including an inactive nitrogen pool (SN_i), an active nitrogen pool (SN_a), and a dissolved nitrate pool

303 (DN). The soil transformations include degradation (Dgd_s , from SN_i to SN_a), mineralisation ($Minr_s$,
 304 from SN_a to DN), denitrification ($Deni_s$, from DN to gaseous N_2), and plant uptake ($Uptk_s$, DN
 305 removal).

$$Dgd_s = SN_i * ref_{Dgd,s} * f_{Ta} * f_{\theta} / dt \quad (30)$$

$$Minr_s = SN_a * ref_{Minr,s} * f_{Ta} * f_{\theta} / dt \quad (31)$$

$$Deni_s = DN * ref_{Deni,s} * f_{Ta} * f_{\theta,deni} * f_{conc,s} / dt \quad (32)$$

306 where $ref_{Dgd,s}$, $ref_{Minr,s}$, $ref_{Deni,s}$ are the parameters representing the reference rates of soil
 307 degradation, mineralisation, and denitrification. f_{Ta} and f_{θ} are the regulating factors of temperature
 308 and moisture.

$$f_{Ta} = 2^{(T_a - 20)/10} * \omega \quad \text{where } \omega = \begin{cases} 1 & T_a > 5 \\ T_a/5 & 0 \leq T_a \leq 5 \\ 0 & T_a < 0 \end{cases} \quad (33)$$

$$f_{\theta} = \min \left[\frac{(1 - p_{\theta,deni}) * (\theta_{fc,i} - \theta_i)}{p_{\theta,fc} * d_i}, \frac{(\theta_i - \theta_{wp,i})}{p_{\theta,wp} * d_i} \right] \quad (34)$$

309 where $p_{\theta,fc}$ and $p_{\theta,wp}$ are the empirical factors that are fixed as 1.2, 0.8 based on literature values
 310 (Lindström et al., 2010; Yang et al., 2018). $p_{\theta,deni}$ is the saturation threshold for soil denitrification
 311 ranging between 0.4 – 0.85 (Yang et al., 2018). A different moisture factor considering a saturation
 312 threshold (θ_{thres}) is employed for denitrification, as denitrification is more sensitive to the soil
 313 wetness condition:

$$f_{\theta,deni} = [(\theta_i / \theta_{fc,i} - \theta_{thres}) / (1 - \theta_{thres})]^{2.5} \quad (35)$$

314 The process is additionally controlled by the concentration level in the storage $f_{conc,s} = C / (C + 10)$.
 315 Plant uptake is simulated using a three-parameter logistic growth equation in (Eckersten et al., 1994;
 316 Lindström et al., 2010).

317 Currently, in-stream denitrification is the only process considered in EcoTWIN.

$$Deni_w = ref_{Deni,w} * f_{Tw} * f_{conc,w} * A / dt \quad (36)$$

318 where $ref_{Deni,w}$ is the reference in-stream denitrification rates. The actual rates are regulated by a
 319 concentration factor $f_{conc,w} = C / (C + 1.5)$ and a temperature factor f_{Tw} (the same equation for f_{Ta}
 320 with inputs substituted by river temperature f_{Tw} , simplified as the rolling-average of 20-day air
 321 temperature).

322 It should be noted that the calibrated soil depth in this study is about 2.5 m, with intermittent
 323 saturation occurring in the deeper layer. This means that terrestrial denitrification is a combination of
 324 soil and groundwater processes in this study, though this might change in other applications if a
 325 shallow soil depth is assigned.

326

327 **3 Model calibration and validation**

328 A robust model application should not only reproduce observed variables through calibration but also
329 yield realistic estimates of internal states and fluxes that are not included in the calibration process.
330 This is essential to avoid situations where inaccurate process representations produce deceptively
331 good results through error compensation. Therefore, we evaluate EcoTWIN from both perspectives.
332 First, we assess the model's ability to reproduce observations via calibration (methods and results in
333 Sections 3.2 and 3.4). Then, we examine the model's capacity to simulate uncalibrated internal states
334 and fluxes by comparing the simulated snow depth, evapotranspiration, and total water storage with
335 corresponding remote-sensing products (methods and results in Sections 3.3 and 3.5).

336 To ensure model generality, 17 catchments were selected for calibration and validation depending on
337 the data availability (particularly stream stable water isotopes and nitrate), which span a wide range
338 of characteristics in geography, climate, and anthropogenic managements (Figure 2 and Table 1).
339 Anthropogenic management practices have a less dramatic effect than climate and geography in most
340 catchments due to the relatively low proportion of urbanized areas. However, a few notable
341 exceptions—such as the Rhine, Elbe, and Danube catchments—are included in the analysis, as these
342 densely populated regions hold critical ecological, agricultural, and economic importance for Europe,
343 and are subject to intensive human interventions in water management. This also provides a chance
344 to examine the applicability of EcoTWIN in human-affected catchments.

345

346 **3.1 Model setup**

347 EcoTWIN was setup for each of the 17 catchments for calibration with a spatial resolution of 5 km²
348 and a temporal resolution of daily timesteps from 1980 to 2024 (with first two years for spin-up). As
349 a fully distributed model, gridded GIS inputs are used in the model setup, including a digital elevation
350 model, flow direction, slope, channel width, channel length, proportion of each land use type (Winkler
351 et al., 2021), proportions of each soil type (world soil map, WRB2014), and soil properties (e.g., depth-
352 dependent proportions of clay, sand, silt, and organic matter from SOILGRIDS). All spatial inputs were
353 acquired with finer resolution (50 m or above) and resampled to the resolution of this application (5
354 km).

355 The climatic variables used to drive EcoTWIN include precipitation, air temperature, potential
356 evapotranspiration, relative humidity, and a few variables that are optional required for the
357 calculation of channel evaporation (air pressure, net radiation, and wind speed). These climatic
358 variables are available from the reanalysis products ERA5 and E-OBS, while PET is calculated using FAO
359 Penman-Monteith equation. For nitrogen simulations, additional inputs are needed including the
360 fertilization map (Grizzetti et al., 2021) and nitrate concentration of rainfall (Zhu et al., 2025) as the
361 boundary of nitrogen addition from agricultural activities and wet deposition.

362

363 3.2 Model calibration

364 **Method.** The calibration was conducted separately for each catchment to test the applicability of
365 EcoTWIN under different geological and climatic contexts. Three commonly used variables for
366 hydrological and water quality modelling (discharge, stream water isotope composition, and in-stream
367 NO₃-N concentrations) are employed for calibration. Their long-term time series were acquired at daily
368 steps from different sources (discharge from GRDC, isotopes from Wateriso and GNIR, and NO₃-N
369 concentration from global water quality database, GEMStat), and then compared with simulation
370 results at multiple sites for each catchment. Here ¹⁸O was selected for isotopic validation due to its
371 higher precision and data abundance. Given the discrepancy in duration of observations (especially
372 for isotopes and NO₃-N), a separate calibration and validation based on a split-sample approach is
373 difficult. Therefore, the full timescale (1982 - 2024) was used for calibration (and the validation
374 introduced in Section 3.3).

375 The DiffeRential Evolution Adaptive Metropolis algorithm (DREAM) was selected for parameter
376 optimisation due to its relatively efficient and effective performance for high-dimensional problems
377 (as benchmarked in Wu et al., 2025c). The algorithm was implemented separately for each catchment
378 with the same prior distribution of parameters (Table S1). The maximum iteration was set as 100,000
379 for each catchment (20 chains with maximum chain length of 5000), from which 40 best simulations
380 were selected from the posterior distribution. The Kling-Gupta efficiency (KGE) statistic was used to
381 construct an informal likelihood function for DREAM optimisation.

$$l = \left[\sum_{i=1}^{N_{obs}} \sum_{j=1}^{N_{site}} (1 - KGE) * w_{i,j} \right]^{-m} \quad (37)$$

382 Where l is the likelihood; N_{obs} and N_{site} are the number of observation types (discharge, isotopes,
383 and nitrate) and sites. The weight $w_{i,j}$, defined for observation type i at site j , is assigned equally
384 across sites such that the total weight for each observation type sums to 1/3. m is an exponentially
385 coefficient to stretch the likelihood surface that is often set based on the number of observation points.
386 After prior test run, m was set as 500. Finally, the likelihood function is transformed to logarithmic
387 form for numeric stability. The calibration was validated using Kling-Gupta efficiency (KGE), Root Mean
388 Square Error (RMSE), Pearson Correlation Coefficient (Coefficient), and Percent bias (Pbias) (Table 2).

389

390 3.3 Model validation

391 **Reanalysis** products were further employed to validate uncalibrated internal model states or fluxes
392 from three important perspectives in ecohydrological modelling — snow depth from ERA5,
393 evapotranspiration from MODIS, and surface water mass anomaly from GRACE (as a storage proxy).
394 The simulated variables corresponding to these products are, respectively, the depth of snow pack,
395 the sum of soil evaporation, channel evaporation, and transpiration from all soil layers, and the
396 anomaly of total water storage above groundwater (i.e., the sum of canopy storage, snow, soil water
397 storages, and unsaturated storage). The validation was realised via resampling the remote sensing

398 ~~products to 5 km and comparing grid to grid with the modelled outputs. Note that r^2 was used as the~~
399 ~~performance metrics, as KGE is not applicable for time series with zero average, yet the average of~~
400 ~~surface mass anomaly is close to 0.~~

402 **3.4 Calibration performance**

403 EcoTWIN successfully reproduced the observed discharge in all 17 catchments with KGE exceeding
404 0.5 at most site (Figure 3a). ~~This is further demonstrated in Figure 4 where both seasonality and peaks~~
405 ~~of discharge with different levels of magnitudes were captured. Such performance is at least~~Such
406 performance is comparable to or better than previous continental calibration of hydrological models
407 (e.g., ParFlow, Naz et al., 2023; E-HYPE, Donnelly et al., 2016).

408 Similarly, isotopic and nitrate simulations also produced good performances at most sites (Figure 3b).
409 However, there are a few exceptions. The failure of isotopic simulations was found at two sites within
410 the Alpine region (bottom left corner of figure 3b). This can be attributed to the uncertainty in
411 precipitation isotopes and snowmelt isotopes (due to the lack of snow elusion fractionation; Ala-aho
412 et al., 2017), the incorrect isotopic composition in groundwater, or the reduced applicability of degree-
413 day model for mountainous areas in Europe. Such simulation deviation due to the uncertainty in data
414 and boundary initialisation is often reported in previous calibration (Smith et al., 2021).

415 In general, the model produces comparable performances to existing nitrogen modelling at catchment
416 (Wu et al., 2022, 2025b; Yang et al., 2018) and continental scales (~~Jones et al., 2023; Mikayilov et al.,~~
417 ~~2015). However, nitrate simulations failed to capture the observations at three sites, though as is~~
418 ~~shown in Figure 4, these all have relatively low levels of NO₃-N concentrations. Such low average~~
419 ~~values can easily trigger the degradation in KGE as one of the sub-components of KGE is highly~~
420 ~~sensitive to the mean deviation, though the absolute deviation remained low (Figure 4, Table 2).~~(Jones
421 et al., 2023; Mikayilov et al., 2015). However, nitrate simulations failed to capture the observations at
422 three sites, though as is shown in Figure S1, these all have relatively low levels of NO₃-N concentrations.
423 Such low average values can easily trigger the degradation in KGE as one of the sub-components of
424 KGE is highly sensitive to the mean deviation, though the absolute deviation remained low (Figure S1
425 and Table 2). Overall, we concluded that EcoTWIN has good capacity to reproduce in-stream
426 components for a wide range of catchments and for relatively long periods.

428 **3.3 Model validation**

429 Method. Remote sensing or reanalysis products were further employed to validate uncalibrated
430 internal model states or fluxes from three important perspectives in ecohydrological modelling – snow
431 depth from ERA5, evapotranspiration from MODIS, and surface water mass anomaly from GRACE (as
432 a storage proxy). The simulated variables corresponding to these products are, respectively, the depth
433 of snow pack, the sum of soil evaporation, channel evaporation, and transpiration from all soil layers,
434 and the anomaly of total water storage above groundwater (i.e., the sum of canopy storage, snow,

soil water storages, and unsaturated storage). The validation was realised via resampling the remote sensing products to 5 km and comparing grid-to-grid with the modelled outputs. r^2 was used as the performance metrics, as KGE is not applicable for time series with zero average, yet the average of surface mass anomaly is close to 0.

Note that all three products may contain considerable uncertainties. ERA5 is a reanalysis product that combines historical observations into global estimates using modelling and data assimilation approaches, therefore inevitably embeds uncertainties associated with model structure and observational coverage (Hersbach et al., 2020). MODIS evapotranspiration is derived from remotely sensed spectral information, energy partitioning approaches and the Penman–Monteith framework, whose uncertainty may exceed 30% depending on spatial scale and environmental conditions (Mu et al., 2011). GRACE infers changes in terrestrially stored water masses from spatial and temporal variations in the Earth’s gravity field; however, its coarse spatial resolution can introduce substantial uncertainty when used for hydrological validation, particularly at basin or sub-basin scales (Tapley et al., 2004). Nevertheless, good agreement between simulations and remote sensing or reanalysis products can enhance confidence in the robustness of simulated spatial and temporal patterns, although it does not necessarily imply accurate representation of absolute magnitudes.

Validation performance

Apart from the variables used for calibration, three internal states and fluxes are also compared with remote sensing products. First, the sum of soil evaporation, channel evaporation, and transpiration was compared to the sum of soil evaporation, channel evaporation, and transpiration to MODIS evapotranspiration in each grid cell. The results in Figure 54 shows a general good fit between simulation and MODIS records with KGE and r^2 above 0.5 in most regions. From the subplots in Figure 54, we can see that the seasonality and magnitude of evapotranspiration were well captured though the peaks in summer were slightly underestimated.

Then, the water storage anomaly was compared to the anomaly of simulated surface storage, i.e., the sum of canopy storage, snow, soil water storages, and unsaturated storage. The grid-to-grid comparison in Figure 64 shows a general good fit in most regions with r^2 close to or above 0.5. However, more degradation was found compared to the performance in evapotranspiration, especially in coastal regions. For instance, GRACE exhibited considerably increasing trends in water storage between 2005 to 2015 in two Nordic catchments (W2 and W3), yet our simulations only showed a moderate increasing trend. Similar degraded performance was found in the coastal catchments (e.g., three British catchments W6-8 in UK), though the magnitudes of simulation and GRACE data fit well. This is possibly attributed to the coarse resolution of GRACE which additionally considered the storage mass from ocean in coastal region yet not included in this terrestrial-explicit modelling.

Finally, the simulated snow depth was compared to the daily snow depth in ERA5 reanalysis products (ERA5 post-processed daily statistics on single levels; 10.24381/cds.4991cf48). Results in Figure 74 show a good agreement between simulations and ERA5 records in most regions with $r^2 > 0.5$, though

473 degradation was found in a few catchments. Note that, the poor performances were generally found
474 in catchments with limited snow accumulation, e.g., W14-17 in subplots in Figure 74. In the other
475 words, the absolute deviation was relatively limited for snow depth simulation.

476

477 **4 Water age simulation and its link to water quality**

478 Like many existing distributed hydrological and water quality models (e.g., SWAT, mHM, EcH₂O-iso,
479 HYPE etc.), EcoTWIN can provide estimation of the main ecohydrological fluxes at high spatial and
480 temporal resolutions, including canopy interception, snow melt-accumulation, infiltration, percolation
481 through soil layers, groundwater recharge, and lateral flux routing at different horizontal phrases.
482 Among these variables, a unique trait of EcoTWIN lies in its capacity to track water fluxes via isotopes,
483 thus being able to provide a consistent estimate of water age and travel times. Therefore, in Figure
484 85, both variables are shown as the long-term average from 1982 to 2024 for soil profile and stream
485 water.

486 Generally, the magnitudes of water ages follow the geographic and climatic gradients, with younger
487 water found in catchments with higher annual precipitation inputs. Those regions locate in the north-
488 west coast of Europe (Figure 25), particularly for Nordic catchments where lower temperature and
489 net radiation further limit the level of potential evapotranspiration, leading to larger percolation to
490 deeper soil layers and groundwater. Such high turnover rates of water in these catchments (W1, W2,
491 W3, W4, W5, and W8) are also demonstrated as the simulated travel time in soil profile with average
492 values remaining below 500 days.

493 A similar pattern was also found in mountainous regions with higher precipitation and lower potential
494 evapotranspiration compared to lowland areas. Two clear examples are W12 and W17 located in the
495 Alps and the Taurus Mountains where water ages and travel time remained below 500 days (Figure
496 25). In specific wet periods, the water ages and travel time can be reduced to just days, suggesting the
497 rapid response of saturated hydrological systems (e.g., the wet year 1999 in Europe in Figure S1-S3S5-
498 7). In contrast, the lowlands in central-west Europe showed much slower turnover rates, with the
499 mean water ages reaching almost 10 years in some specific regions. A few examples could be found
500 in the three major representative catchments in Central Europe – Elbe, Rhine, and Danube (W9-11).
501 Such old water ages and long travel time are further exacerbated during dry years (e.g., 2004, a
502 drought year for much of Europe shown in Figure S1-S3S5-7).

503 Note that though water ages and travel time share similar magnitudes and spatial patterns. It is partly
504 attributed to the fact that the travel time in the conceptualised storages increases exponentially in a
505 sequential order. Taking the Rhine as an example, the average travel time in top soil layer, median soil
506 layer, deep soil layer are 65, 225, 1291 days, respectively. Such a depth-dependence profile makes the
507 overall ages/travel time follow the magnitude of bottom layer and leads to similarity between water
508 ages and travel time. However, large discrepancies are possible between the two indices if a shallow
509 lower boundary is adopted.

510 The estimation of travel time and water ages further provides opportunities to link hydrology and
511 water quality processes in the modelling framework. The simplest and most intuitive way is to
512 compare travel times and simulated biogeochemical process kinetics. Taking denitrification as an
513 example, we applied linear regression and Spearman's correlation test to investigate the potential
514 correlation between travel time of soil water and denitrification rates. The results in Figure 96 showed
515 the strong positive correlations in most agricultural-dominated catchments (W5, W5, W6, W8, W9,
516 W11) yet only weak or no correlation in remaining pristine watersheds. This suggests that travel time
517 might be a key control on soil nitrogen removal in European croplands.

518 More insights can be gained via examination of the Damköhler Number, which quantifies the ratio
519 between timescales of solute transport and biogeochemical transformation. Here in our modelling
520 framework, it can be calculated as the ratio between the travel time of soil water and the time for all
521 soil NO₃-N storage to be removed under the simulated denitrification rates. Damköhler numbers <1
522 mean that soil water nitrogen cannot be fully removed during time of residence, indicating the
523 dominance of transport over removal processes and the potential of nitrogen leaching. As shown in
524 Figure 107c, the long-term averages of Damköhler number remain below 1 in most croplands,
525 supporting the conclusion from the linear regression (travel time is a major limiting factor on soil
526 nitrogen removal). Via the spatial- and temporal-explicit estimation of Damköhler number, EcoTWIN
527 provides the opportunity to bridge the catchment hydrological and water quality with travel time.

528

529 **5 Discussion**

530 **5.1 Structural and Functional Merits of EcoTWIN**

531 As a new tracer-aided ecohydrological model, EcoTWIN has novel advantages compared to previous
532 models. In this section, we briefly introduced the merits in model structure, applicability, and insights
533 from tracer-aided simulation.

534 **5.1.1 Integrated C++ framework**

535 Applications of large-scale modelling have been increasingly popular due to the accelerating
536 development of observation networks and availability of remote sensed data. However, it severely
537 increases the computational burden of ecohydrological modelling. Especially for fully distributed
538 models, increasing size of the model domain can lead to exponential increase in computation demands.
539 In this context, an integrated framework in C++ can significantly accelerate the modelling tasks, as all
540 computation can be conducted within memory thereby avoiding the additional input/output
541 overhead associated with disk-based operations in loosely coupled model chains (e.g., ECH₂O-iso-
542 nitrate; Yang et al., 2024). A standard test was not performed, but based on our modelling experience
543 in the same catchment with different models, the speed of EcoTWIN (~5 seconds for a simulation with
544 285 grid cells and 30 years at daily timestep) is close to the water quality model mHM-Nitrate (~5
545 seconds yet without isotopic simulations; Wu et al., 2022) and easily outperforms ECH₂O-iso-nitrate (7
546 minutes; Wu et al., 2025b).

547 **5.1.2 Selective disassembly structure**

548 EcoTWIN incorporates a wide range of ecohydrological processes from canopy to groundwater, which
549 not only include natural processes but also anthropogenic activities like irrigation. Land managements
550 can also be represented by dynamic parametrisation, thus enabling EcoTWIN to function as a learning
551 tool to investigate the impacts of changes in anthropogenic management over natural ecosystems;
552 for instance, the land use distribution was updated every 10 years in our test examples to reflect the
553 moderate increases in afforestation in the past 45 years in Europe. More importantly, unlike hard
554 coded process representations/equations in most ecohydrological models, EcoTWIN has a selective
555 disassembly structure, which provides alternative conceptualisations for several important hydrological
556 processes (canopy interception, percolation, groundwater recharge, as well as three pedotransfer
557 functions for initialising soil properties). Modellers can benefit from such flexible model structures by
558 either selecting process representations best suited to field knowledge or data prior to calibration, or
559 integrating module selection into the calibration thus enabling simultaneous optimisation of model
560 structure and corresponding parameters. The latter aspect, i.e., the optimisation of model structure,
561 can be realised together with the recently developed optimisation algorithm DREAM_(LOAX) that aims to
562 identify the deficits in model structure during calibration (Wu et al., 2025a).

563 **5.1.3 Transferability to contrasting geographic and climatic contexts**

564 To thoroughly test the applicability of EcoTWIN, 17 catchments with different climatic and
565 geographical contexts were selected for calibration and validation, spanning over most biomes in
566 Europe, from snow-dominated watersheds in Nordic or alpine regions, to agricultural-influenced
567 lowlands catchments, and Mediterranean ecosystems (Figure 12 and Table 1). Through multi-criteria
568 calibration against three objectives at multiple sites, the model successfully reproduced the
569 seasonality and peaks of discharge, in-stream isotopes, and NO₃-N concentrations in most catchments.
570 Such performance is comparable or better than the previous model benchmarks at similar scales
571 ([Bajracharya et al., 2023](#); [Mikayilov et al., 2015](#); [Rakovec et al., 2016, 2019](#)) ([Bajracharya et al., 2023](#);
572 [Mikayilov et al., 2015](#); [Rakovec et al., 2016, 2019](#)). Note that the concentration of NO₃-N was used for
573 calibration, whose accurate simulation is more difficult than NO₃-N loads given the naturally good
574 performance in discharge. In the other words, hydrological simulation is often the least problematic
575 part in integrated water quality modelling, as it is mostly dominated by natural catchment properties
576 while nitrogen cycling is more interfered by anthropogenic managements (e.g., fertilization and
577 irrigation) (Wu et al., 2025b). Additionally, the simulated internal fluxes were also compared to three
578 reanalysis products in hydrological simulations, corresponding to the key fluxes or storage states in
579 hydrological cycling (snow melt-accumulation, evapotranspiration, and water storage). The results
580 show that constrained by isotopes, EcoTWIN was able to reproduce comparable hydrological
581 modelling results to the remote sensing [observationsdata](#) without direct calibration regarding
582 magnitudes, spatial patterns, and temporal dynamics. The only degraded performance was found in
583 GRACE surface mass anomaly in coastal regions. There are two potential reasons: (i) the coarse
584 resolution of GRACE might account for mass shifts in both ocean and land, yet EcoTWIN only produces
585 mass anomaly in terrestrial systems; (ii) bidirectional fluxes across the land-ocean interface might

586 drive key changes in coastal systems, which is not considered in current version of EcoTWIN.
587 Nonetheless, given the relatively good agreement with most available [observations data](#), we conclude
588 that EcoTWIN is applicable across a range of terrestrial ecosystems from boreal to temperate and
589 subtropical climate.

590 ***5.1.4 Bridging hydrology and water quality with water ages***

591 Further to the inference of hydrological and nitrogen processes that is also available in other
592 distributed water quality models (Wellen et al., 2015), a unique trait of EcoTWIN lies in its capacity to
593 track water fluxes and ages with stable water isotopes. As a tracer-aided model, EcoTWIN not only
594 simulates the celerity of catchment response, but tracks the velocity of water via different flow paths.
595 The importance of delineating flow paths within catchments has long been recognized by hydrologists,
596 and has motivated the development of many indices to describe the movement of water molecule at
597 catchment-scale and estimate associated timescales (Sprenger et al., 2019). A few examples are water
598 ages, transient time distribution, and young water fractions (Benettin et al., 2015; Hrachowitz et al.,
599 2013; Jasechko et al., 2016). However, those indices are mainly calculated in a lumped manner where
600 different flow paths in the catchment are characterised as a black box, thus characterising the overall
601 input-output dynamics yet potentially omitting important spatio-temporal variability of hydrological
602 boundary conditions. Instead, EcoTWIN, benefiting from the gridded-based structure, can utilise the
603 increasingly available spatial information (e.g., gridded remote sensing datasets) thus characterising
604 the water ages and travel time in a spatially-explicit manner. Note that simulations of water age/travel
605 time, like other ecohydrological processes, are sensitive to spatial resolution. The coarse resolution
606 used for large catchments (e.g., 5 km in this study) may obscure the sub-grid heterogeneity. For
607 instance, local hydrological hotspots characterized by short travel times and young water ages can be
608 damped or averaged out at coarser resolutions, as reported in modelling studies using ECH2O-iso
609 (Smith et al., 2021; Yang et al., 2023b). However, this limitation can be mitigated by increasing spatial
610 resolution, and it does not undermine the utility of EcoTWIN for water-tracking.

611 Compared to water age which quantifies the age of water within the overall system, travel time,
612 accounting for the water age within a specific storage, is more important in understanding the links
613 between hydrological and nutrient cycles. Such an index, also known as transit time or exposure time,
614 forms one of the fundamental components of water quality modelling. Therefore, the travel time
615 estimated by EcoTWIN has potential to improve the simulation of biogeochemical transformations in
616 water quality models interfaced with simplified hydrological modules (e.g., MONERIS; Bonchkovsky
617 & Osadcha, 2024). Moreover, travel time can be used as a proxy to bridge hydrological processes and
618 biogeochemical transformations. Here we presented a simple framework to calculate the Damköhler
619 Number for denitrification. By using the simulated travel time and reaction timescale (i.e., the time
620 for full removal of nitrogen storage under current denitrification rates), estimation of Damköhler
621 Number was achieved in a spatially- and temporally-explicit manner (Figure 97), which can highlight
622 where and when soil nitrogen removal is constrained by the limited exposure time in the catchment.
623 Such high-resolution information is unique, as the use of this index has been largely restricted to

624 steady-state groundwater systems or riparian/hyporheic zones due to the difficulty in quantifying
625 processing time and residence time at larger scales (Ocampo et al., 2006; Wu et al., 2022).

626

627 **5.2 Limitations and roadmap for future development**

628 Despite these advances, EcoTWIN has limitations. In this section, the uncertainties in model structure
629 and conceptualisation are introduced, as well as the potential roadmaps for future developments.

630 ***5.2.1 Potential towards physics-based conceptualisation of groundwater***

631 Groundwater in EcoTWIN is characterised as two conceptual storages linking with adjacent upstream
632 and downstream storages following the topographic gradients. Such conceptualisation, although has
633 been widely employed in hydrological models (e.g., SWAT, mHM, ECH2O, STARR, etc.), does not align
634 with the physical mechanisms of groundwater routing, as groundwater flow direction follows the
635 hydraulic gradients which may not entirely coincide with topographic gradients (Condon et al., 2021).
636 Such simplified routing has less effect in large catchments with clear topographic gradients (e.g., Rhine
637 starting from Alps to North plain), yet might cause biased estimation in water mass balance for flatter
638 headwater catchments (Yang et al., 2025). Therefore, we plan to further incorporate an additional
639 groundwater module to realise physics-based routing following Darcy's Law in future.

640 ***5.2.2 Revisiting mixing strategies***

641 Mixing strategy is a key component in water quality or tracer models describing the flux-storage
642 behaviours along specific flow paths. There has long been a debate on different mixing assumptions
643 and theories. A typical example is the two-water-world hypothesis, where water storage in the soil
644 profile is differentiated into a tightly-bound pool and a mobile-water pool (McDonnell, 2014). Such
645 conceptualisation is close to the definition of soil matrix flow and preferential flow: the existence of
646 free-flowing preferential flow will bypass the soil matrix vertically and accelerate the lateral drainage
647 via direct connection with channel network (Hrachowitz et al., 2013; Sprenger et al., 2019). However,
648 a complete mixing strategy is often regarded as a reasonable first approximation in many situations
649 and is used in most water quality and tracer models (Jung et al., 2025). This is not only attributed to
650 its computational simplicity, but also the difficulty in conceptualising preferential flow in an
651 evidenced-based manner. In the other words, even with the recognition of preferential flow, its
652 calculation is often hindered by the subsurface heterogeneity in soils and bedrock; a good visualisation
653 is given in Figure 7 in Sprenger et al., (2019). Alternatively, partial mixing has been developed for
654 ecohydrological models (e.g., Hrachowitz et al., 2013), which could be added as a complementary
655 mixing strategy in EcoTWIN. However, as benchmarked in Hrachowitz et al., (2013), the partial mixing
656 brings only moderate improvements in simulations yet can introduce challenges to model spin-up (the
657 increasing instability of storage ages due to the exchange between bypass and storage compartment).
658 Moreover, the realisation of partial mixing, like preferential flow, relies on additional parameters to
659 describe the timing and extent of mixing thus introducing additional parametric uncertainty.

660 Therefore, we recommend a rigorous evaluation of the necessity of partial mixing before any
661 application.

662 ***5.2.3 Complementing the in-stream biogeochemical processes***

663 Transformation is as crucial as transport in inland-water nitrogen cycling (Wang et al., 2024). In the
664 current version of EcoTWIN, denitrification is the only in-stream process of nitrogen loss. However,
665 recent studies have shown that other processes are involved which may be important for aquatic
666 nitrogen cycling. An example originates from Wang et al., (2024), where global inland-water modelling
667 shows that in-stream denitrification only accounts for a minor fraction of NO₃-N removal compared to
668 biological uptake. Though their modelling considers lakes and reservoirs where primary production of
669 benthic plants and algae is usually greater than that in rivers, in-stream assimilation might still play a
670 significant role, particularly, in slow-flowing river systems. This is supported by a recent modelling
671 study that estimated nitrogen retention at 15-min interval based on high-frequency NO₃-N data (Yang
672 et al., 2023a). Therefore, we plan to further compliment EcoTWIN with in-stream assimilation
673 conceptualisation, as well as other potentially important riverine processes (e.g., nitrogen burial in
674 sediments; Akbarzadeh et al., 2019).

675 ***5.2.4 Integrated calibration framework to embrace equifinality***

676 Strictly speaking, equifinality is not specifically linked to EcoTWIN, but remains a universal problem for
677 calibration or parameter tuning for almost all ecohydrological models. It is reflected in multiple
678 parameters sets yielding similarly good model performance, thus increasing the uncertainty in process
679 inference. The extent of equifinality is primarily controlled by the magnitude of parameters and
680 observation/objectives (Wu et al., 2025c). Unfortunately, conceptualisations across diverse process
681 domains (e.g. for hydrology, isotopes and N-cycling) in EcoTWIN also lead to a relatively large number
682 of parameters. Such risk in equifinality can be potentially constrained via sensitivity analysis, but can
683 still remain an issue given the ubiquitous epistemic uncertainty in data and model structure (Beven,
684 2006, 2015). Alternatively, the recently developed calibration algorithm DREAM_(LoAx) provides an
685 opportunity to embrace equifinality by tuning parameters based on the limits-of-acceptability theory
686 under the equifinality thesis (Wu et al., 2025a). The integrated modelling framework of EcoTWIN and
687 DREAM_(LoAx) can potentially increase the robustness of model calibration and inference.

688

689 **6 Conclusions**

690 Uncertainty is a central concern in ecohydrological modelling, as models are not only used for
691 prediction of specific variables, but also for process inference (backtracking internal processes from
692 available observations) that are inherently embedded within considerable uncertainty. Stable water
693 isotopes can help effectively constrain hydrological fluxes due to their conservative nature, motivating
694 the increased development of tracer-aided models. However, few attempts have been made to
695 incorporate a tracer-aided hydrological framework into water quality models.

696 Therefore, we introduced EcoTWIN, a fully distributed tracer-aided **ecohydrological** model that **tracks**
697 **water**, **isotopic**, and **nutrient** fluxes simultaneously in an integrated C++-based framework. To
698 thoroughly validate the model, 17 large European catchments were selected with a wide range of
699 geographic and climatic gradients (from snow-dominated watersheds in Nordic or alpine regions, to
700 agricultural-influenced lowlands catchments, and Mediterranean ecosystems). The model was
701 calibrated against long-term observations of discharge, in-stream isotopes, and NO₃-N concentrations
702 during 1980-2024 in each of the 17 catchments. Additionally, uncalibrated internal states and fluxes
703 were also compared with three remote sensing products (ERA5 snow depth, MODIS
704 evapotranspiration, and GRACE surface water anomaly) to validate the credibility of process inference.

705 The generally good agreements in both calibrated in-stream components and uncalibrated internal
706 flux-states demonstrated that EcoTWIN is a transferable, flexible prediction and learning tool for
707 process inference across biomes ranging from boreal to subtropical climate. Constrained by tracer
708 simulations, the model not only reproduces the celerity of hydrological systems, but also tracks the
709 velocity. Water ages and travel time are embedded in EcoTWIN to provides spatio-temporal-explicit
710 insights into *when*, *where*, and *how* water moves in the system. Such indices further provide the
711 opportunities to efficiently bridge hydrology and water quality at large catchment-scales. An example
712 was presented using the Damköhler Number to identify regions where denitrification was limited by
713 fast turnover rates of water.

714 Following this “proof of concept” we also see numerous areas where future developments can
715 improve the limitations in the 1.0 version of the model.

716

717 **Code and data availability**

718 The initial version (v1.0) of EcoTWIN is archived in <https://doi.org/10.5281/zenodo.16747633> (Wu et
719 al., 2025d). For further development please refer to GitHub repository: [https://github.com/songjun-
720 wu/EcoTWIN](https://github.com/songjun-wu/EcoTWIN). The geographic data were acquired from Catchment Characterisation and Modelling
721 database (CCM2, version 2.1). The climatic forcing was acquired from E-OBS database
722 (<https://www.ecad.eu/download/ensembles/ensembles.php>). The LAI were acquired from MODIS
723 database (<http://doi.org/10.5067/MODIS/MOD15A2H.006>). Long-term observation of discharge was
724 acquired from GRDC (<https://grdc.bafg.de/>); in-stream isotopic observations were available from
725 Wateriso database (<https://wateriso.utah.edu/waterisotopes/index.html>) and GNIR database
726 (<https://www.iaea.org/services/networks/gnir>); In-stream NO₃-N concentration were acquired from
727 global water quality database, GEMStat (<https://gemstat.org/>).

728

729 **Acknowledgements**

730 Tetzlaff's and Wu's contributions were partly funded through the WETSCAPES2.0 project (DFG
731 TRR410/1 2025) and the Einstein Research Unit “Climate and Water under Change” from the Einstein
732 Foundation Berlin and Berlin University Alliance (grant no. ERU-2020-609). Tetzlaff was also partly

733 funded through Leibniz Excellence project ISOSCALE and received funding from the
734 “Wasserressourcenpreis 2024” of the Rüdiger Kurt Bode-Foundation. This research was also
735 supported by the BMBF (funding code 033W034A), which supported the IGB stable isotope Laboratory.
736 Contributions from Soulsby were supported by Leibniz Association Germany in the project Wetland
737 Restoration in Peatlands.

738

739 **Author contribution**

740 Conceptualization: SW, DT, YZ, CS

741 Data curation: SW

742 Methodology: SW

743 Software: SW

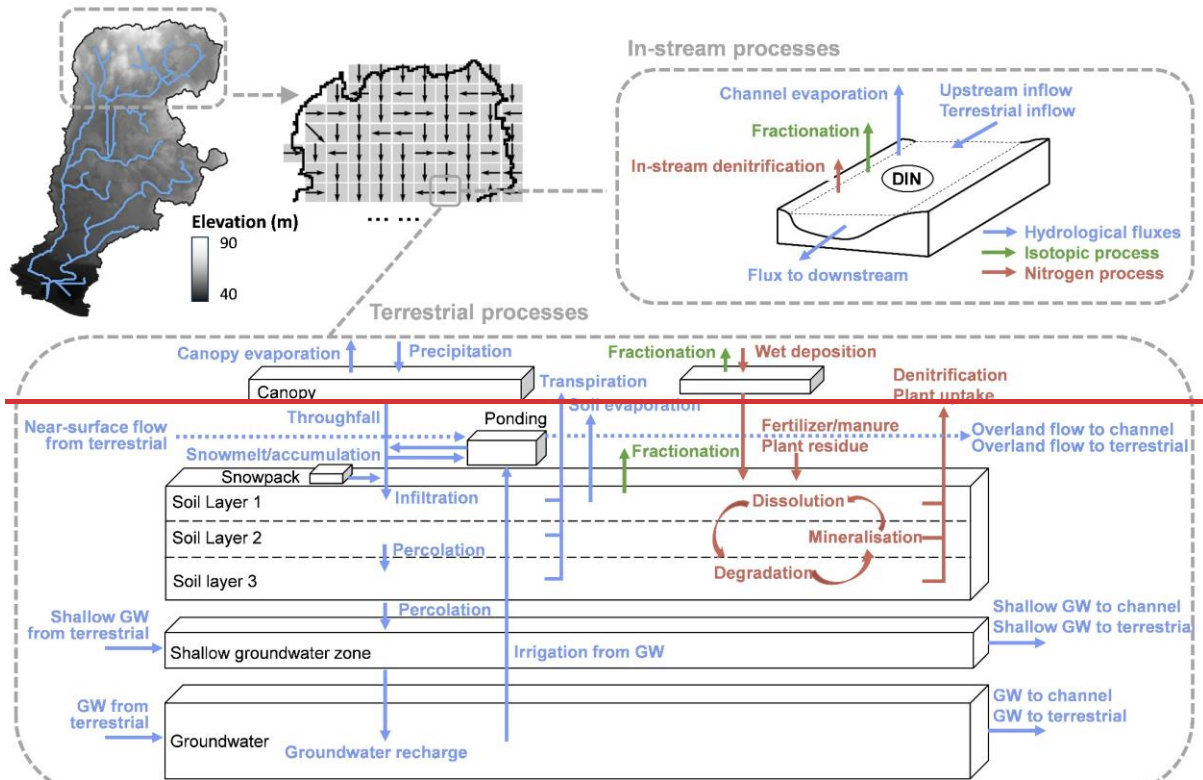
744 Investigation: SW, DT, YZ, CS

745 Visualization: SW

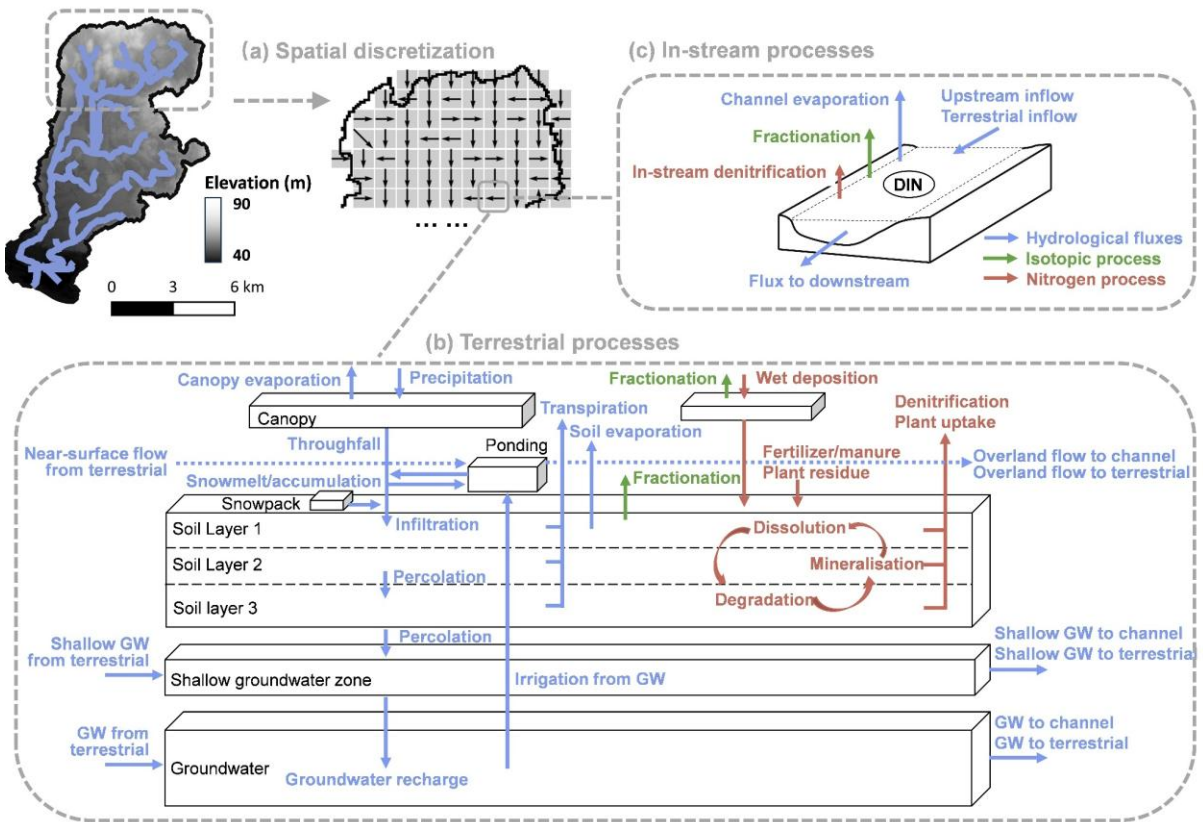
746 Supervision: DT, CS

747 Writing (original draft preparation): SW

748 Writing (review and editing): SW, DT, YZ, CS



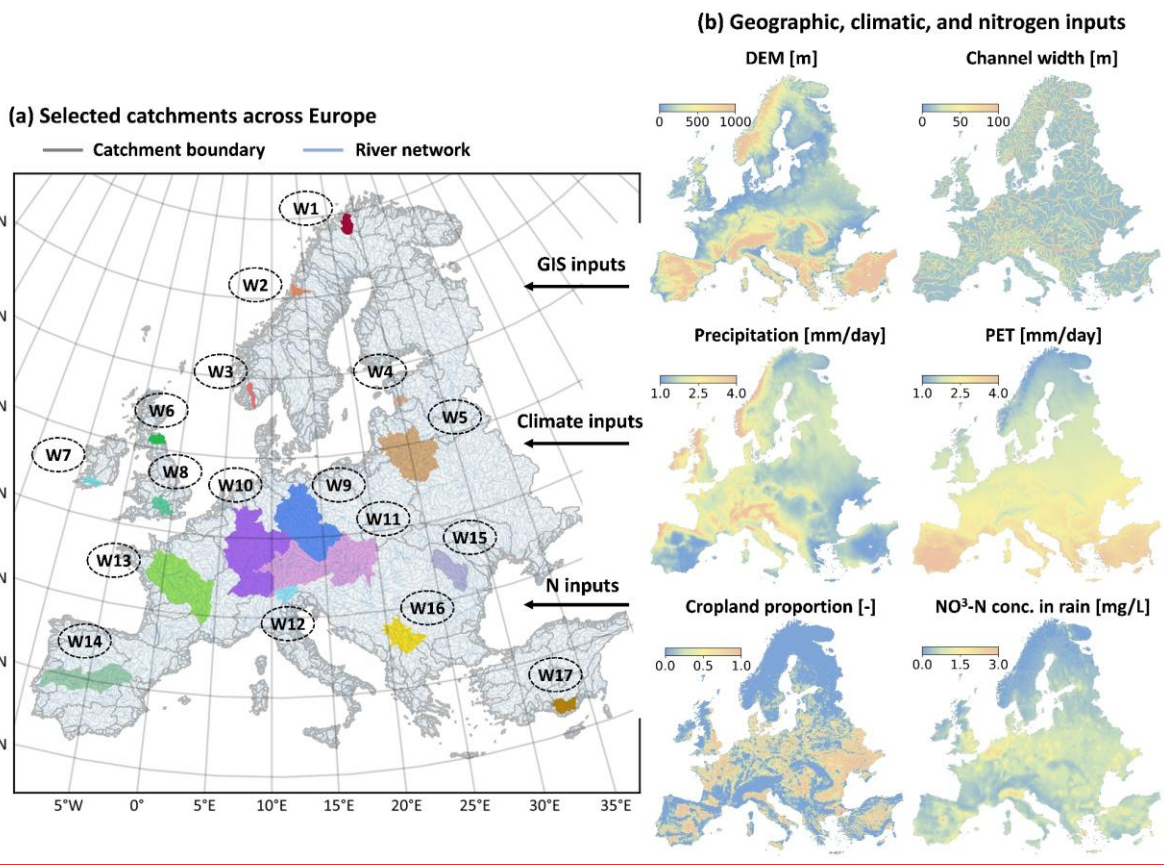
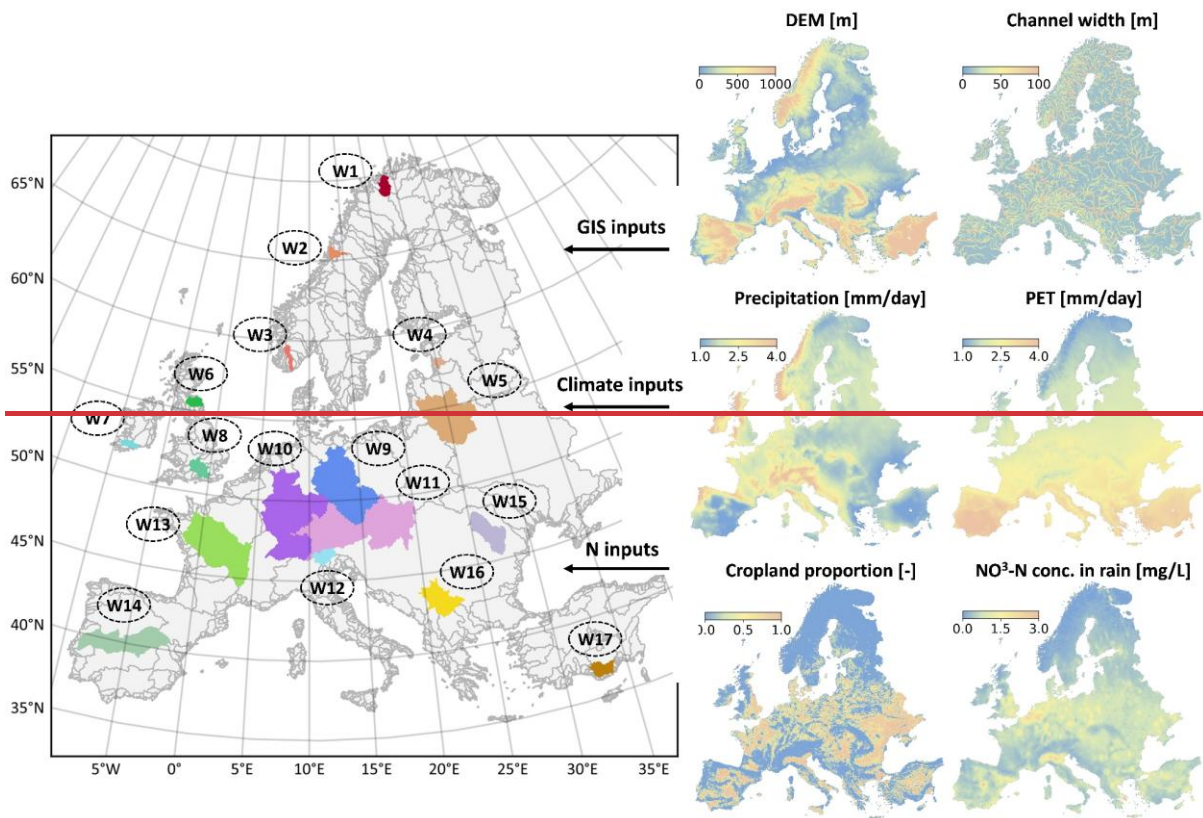
751



752

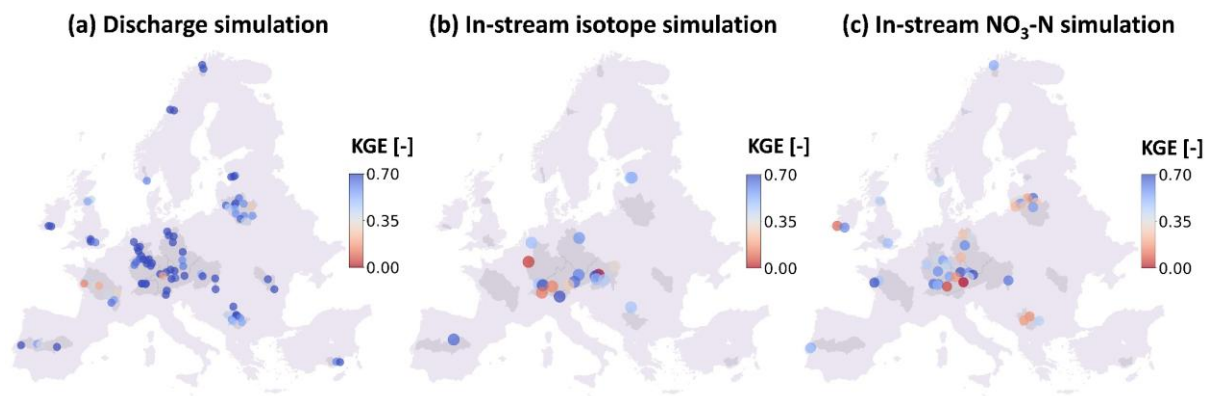
753 Figure 1. Model structure of EcoTWIN. As a distributed model, EcoTWIN disentangles the spatial
754 domain into grid cells. (Panel a). In each grid cell, hydrological, isotopic, and nitrogen processes were

755 simulated in canopy, snow, soils, shallow groundwater, and groundwater (panel b) and river channel-
756 if channels are present (Panel c).
757



761 Figure 2. The selected catchments for model validation ([Panel a](#)) and an overview of key [geographic,](#)
762 [climatic, and nitrogen](#) inputs- ([Panel b](#)).
763

764

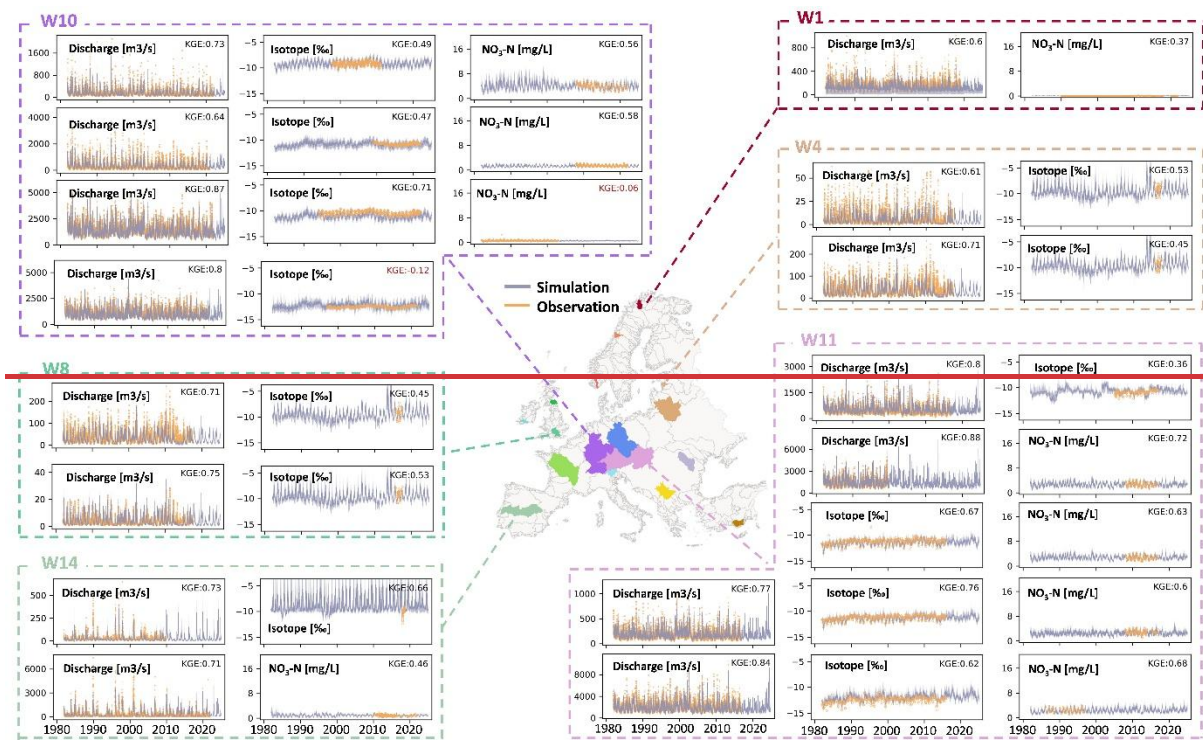


765

766

Figure 3. The simulation performance of discharge, in-stream isotope, and in-stream NO₃-N.

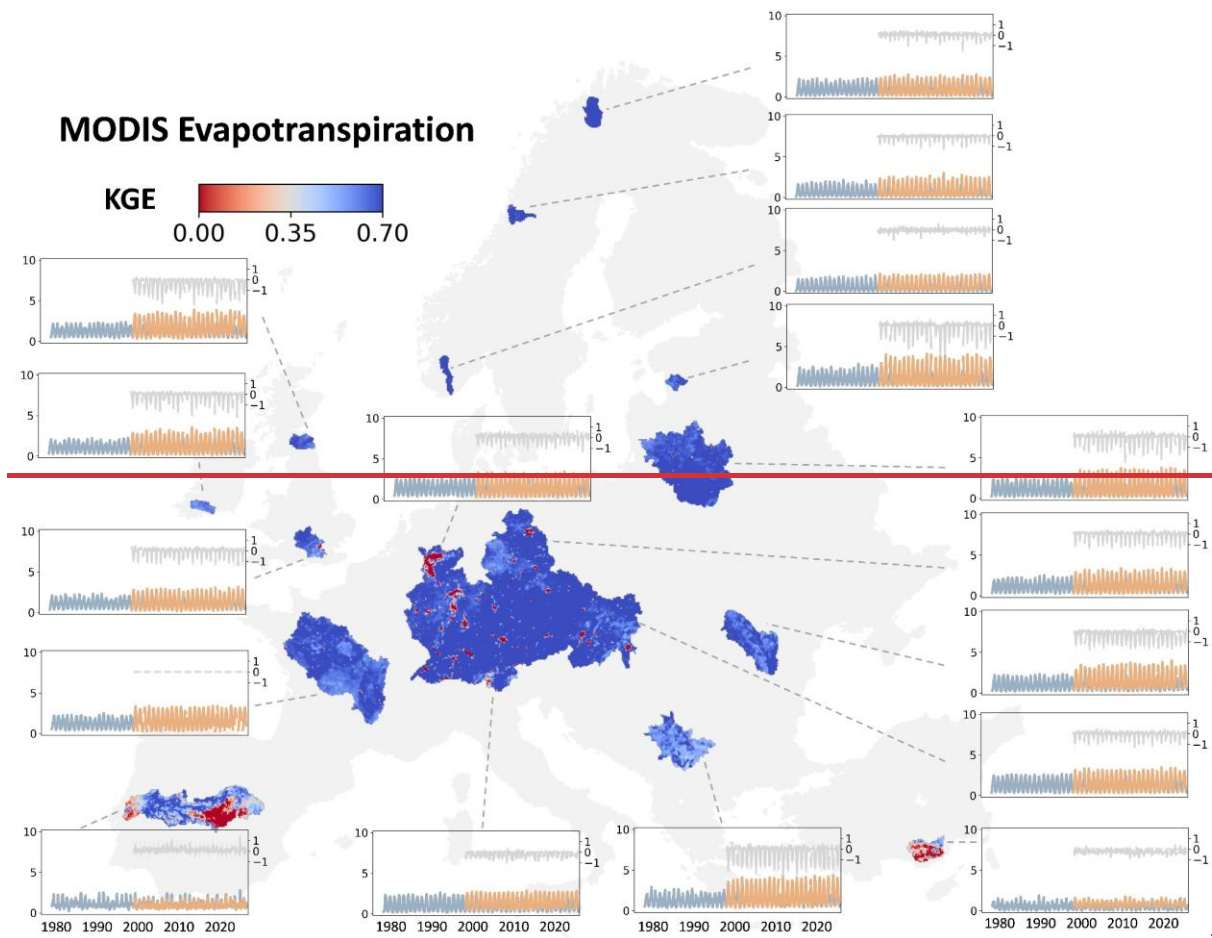
767



769

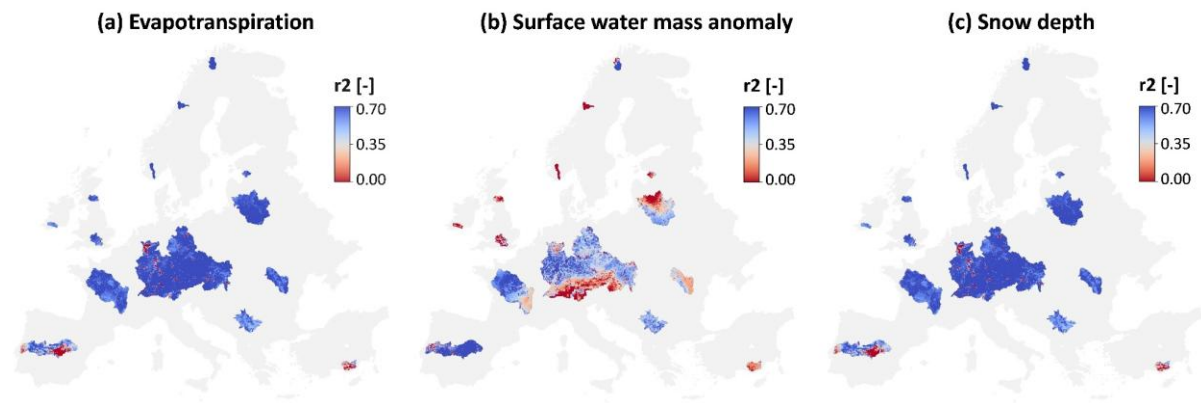
770 Figure 4. The simulated (blue) and observed (orange) time series of discharge, isotopes, and $\text{NO}_2\text{-N}$ at
 771 representative gauges. Note that the sites with relatively poor performance ($\text{KGE} < 0.2$) were
 772 particularly shown for model diagnosis.

773 [time series are shown in Figure S1.](#)



774

775

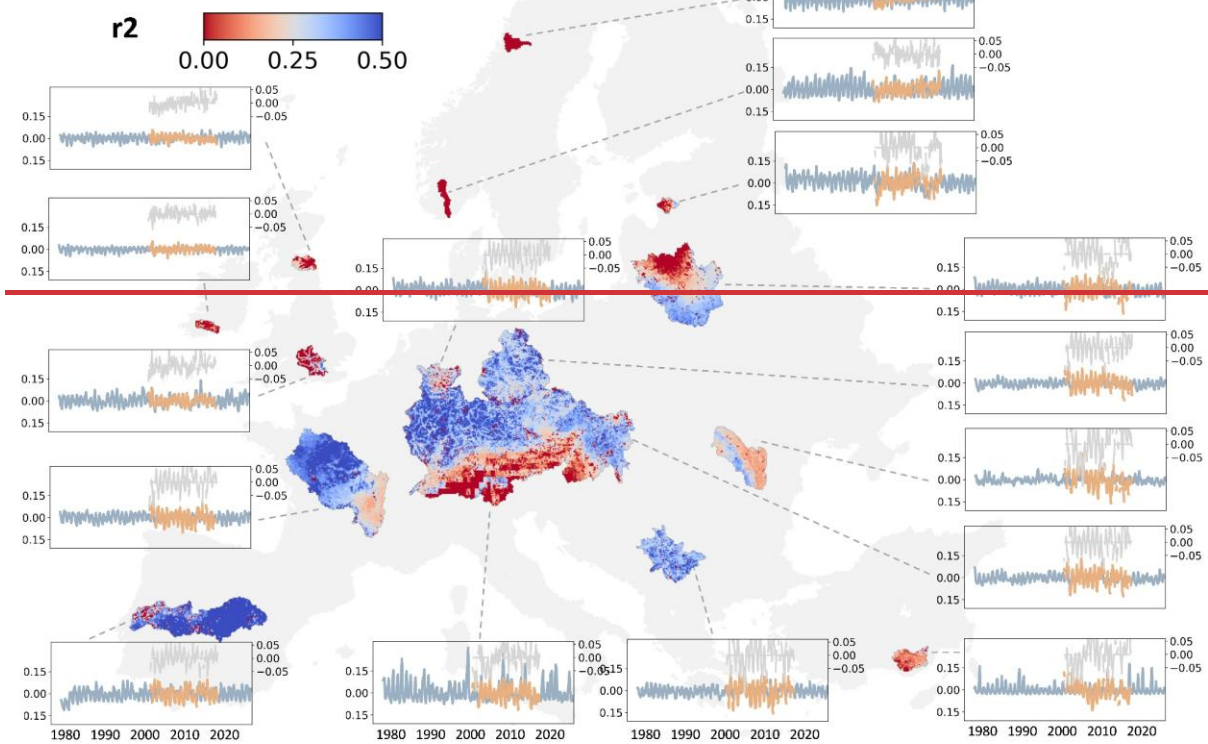


776

777 Figure 54. The grid-to-grid comparison between time series of simulated internal states/fluxes and the
 778 ones extracted from remote sensing/reanalysis products, including evapotranspiration and from
 779 MODIS evapotranspiration shown in KGE. The time series in inset subplots show the monthly dynamics
 780 of simulated (blue) and observed (orange) values averaged from all grid cells in the watershed, as well
 781 as their deviations (grey).

782

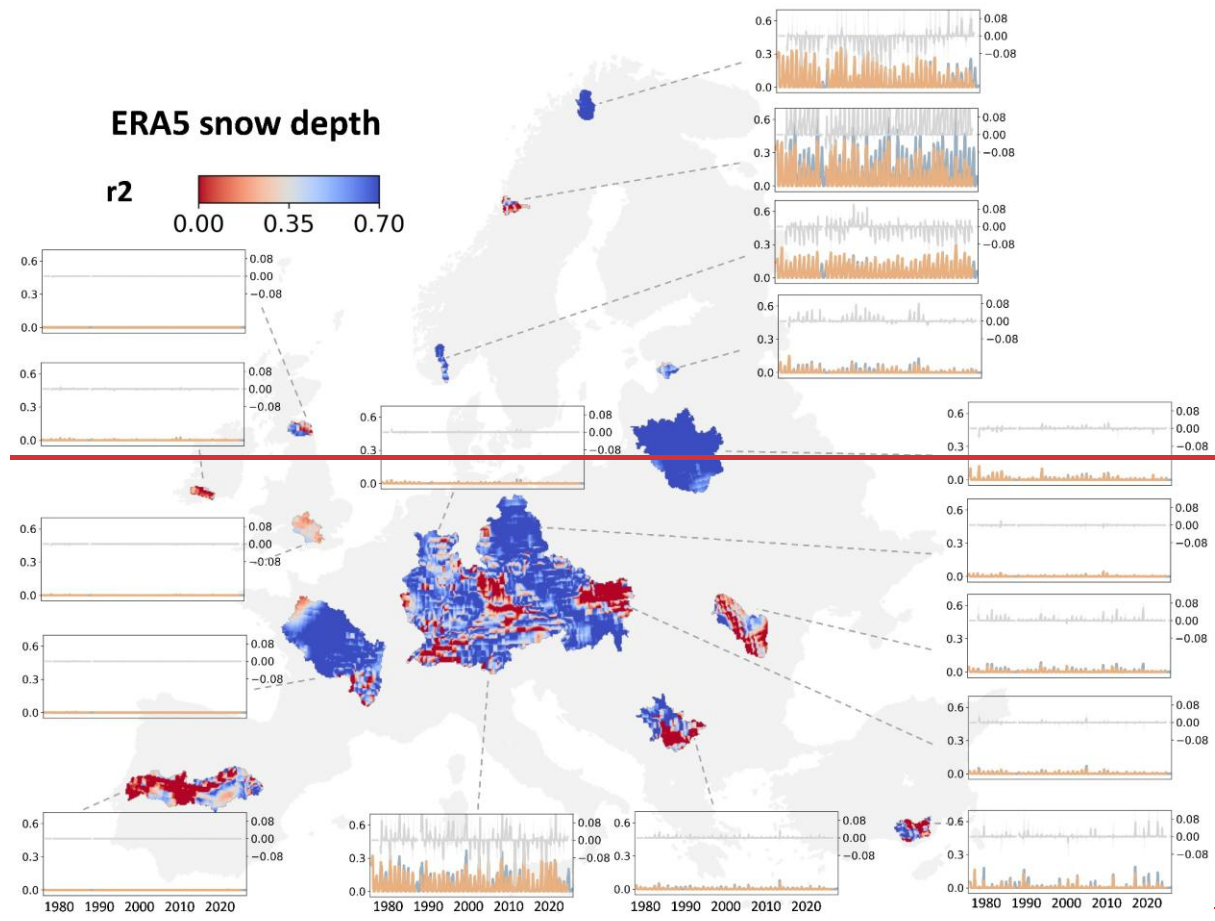
GRACE surface water mass anomaly



783

784 Figure 6. The grid-to-grid comparison between simulated water storage anomaly and GRACE (Panel a),
785 surface water mass anomaly from GRACE (Panel b), and snow depth from ERA5 (Panel c). The time
786 series show the monthly dynamics of simulated (blue) and observed (orange) values averaged from
787 all grid cells in the watershed, as well as their deviations (grey) of simulation and remote
788 sensing/reanalysis products in each catchment are shown Figure S2-4.

789



790

791

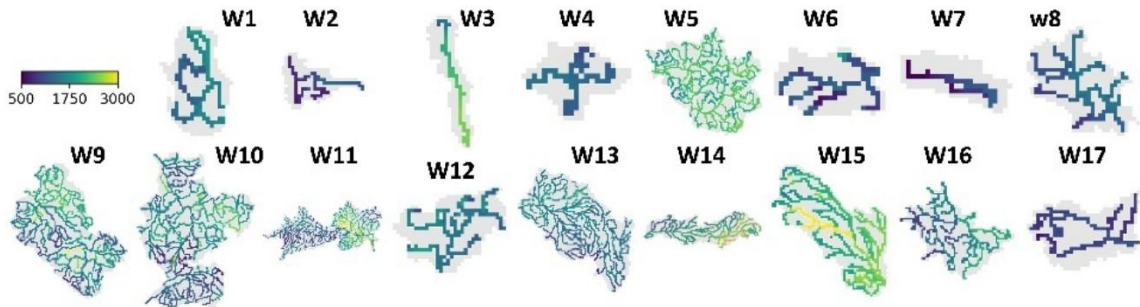
792

793

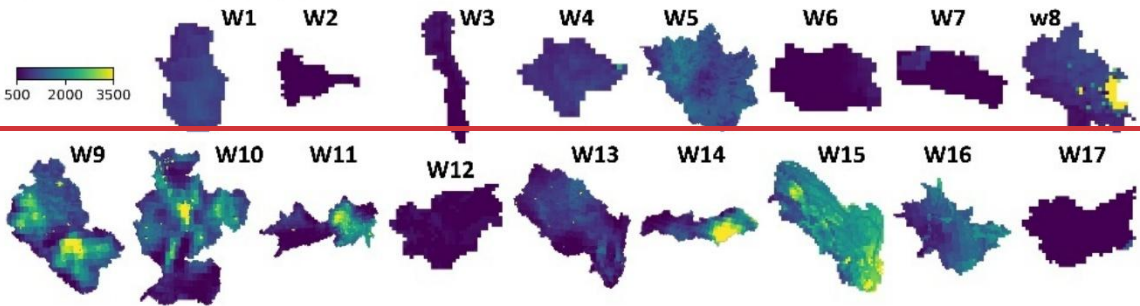
794

Figure 7. The grid-to-grid comparison between simulated snow depth and ERA5 snow depth. The time series show the monthly dynamics of simulated (blue) and observed (orange) values averaged from all grid cells in the watershed, as well as their deviations (grey).

(a) Stream water age [days]



(b) Soil water ages [days]



(c) Travel time in soils [days]

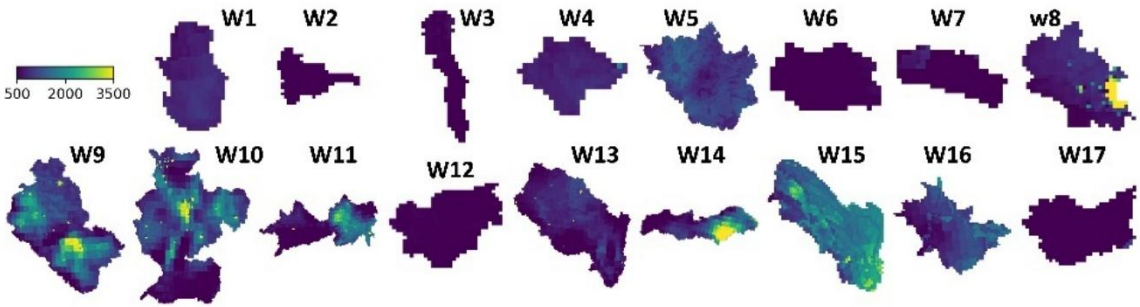
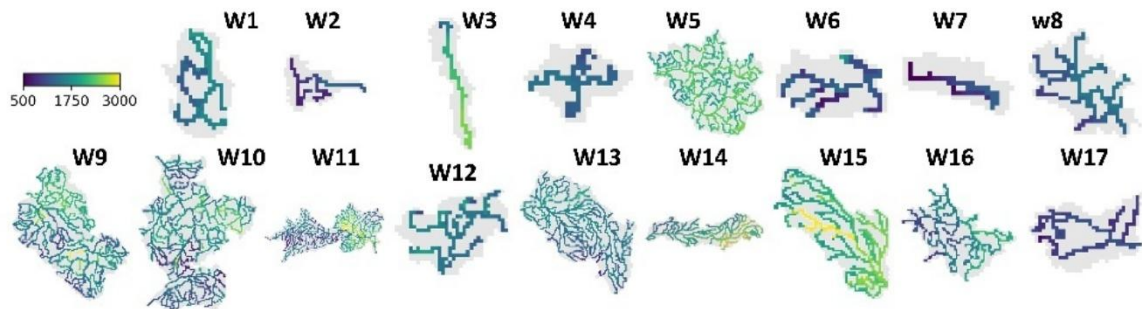
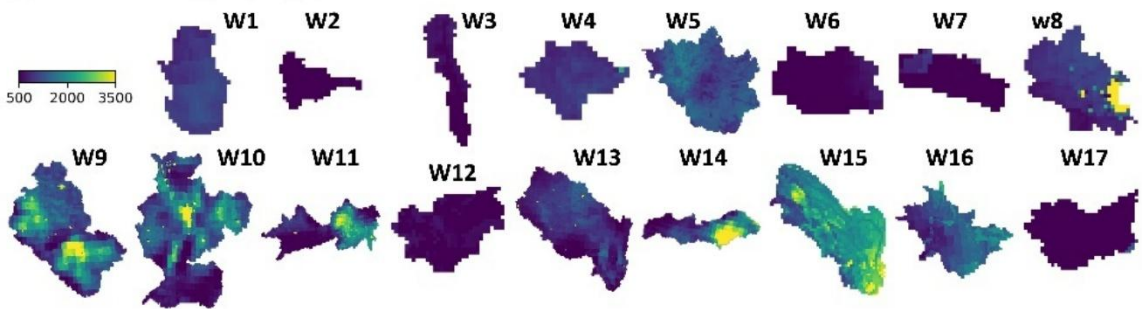


Figure 8.

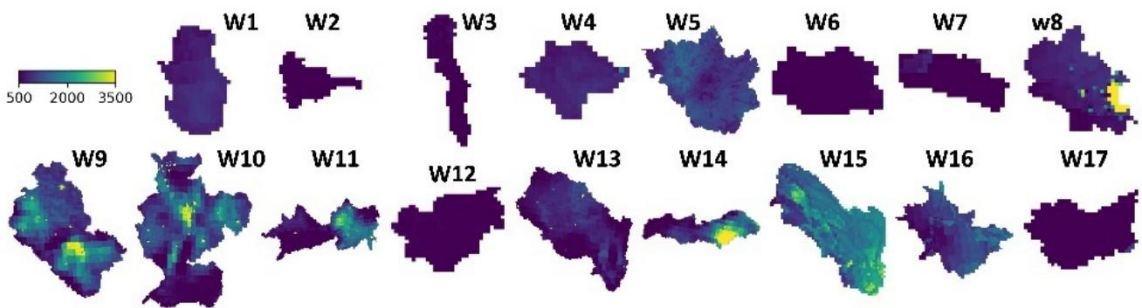
(a) Stream water age [days]



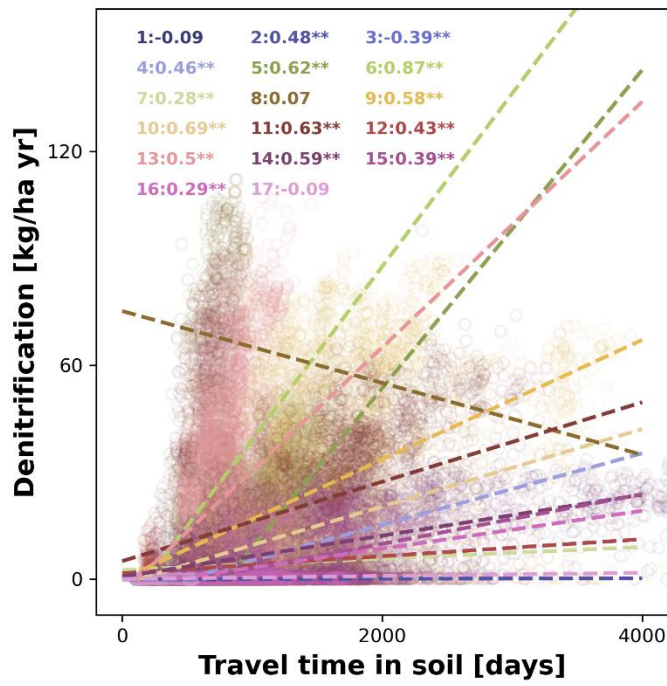
(b) Soil water ages [days]



(c) Travel time in soils [days]



800 **Figure 5.** The simulated long-term average (1982-2024) of water age and travel time in channel and
801 soil profile. Water ages represent the time since water enters the catchments as precipitation, while
802 travel times depict the residence time of water within the specific storage.

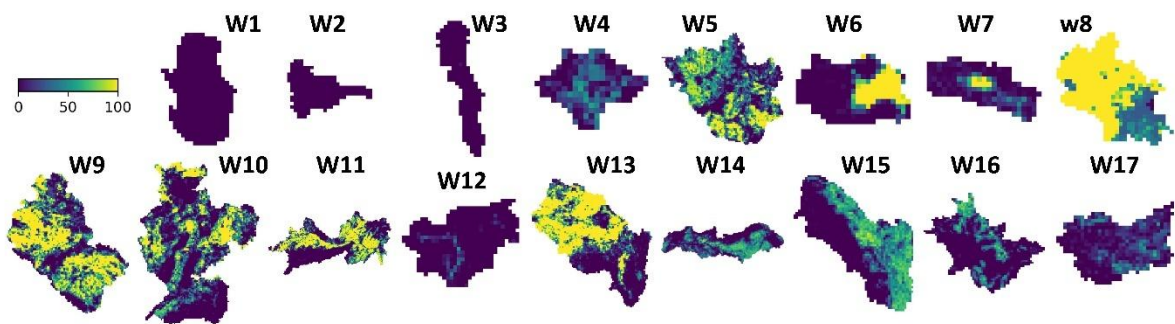


804

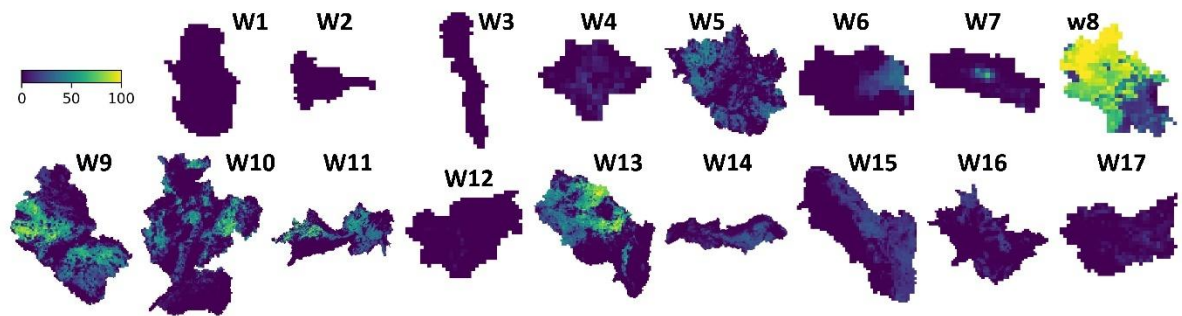
805 Figure 96. The correlations between travel time and annual denitrification. The text depicts the
 806 spearman correlation coefficients and p values (* = less than 0.05, ** = less than 0.01) in each
 807 catchment.

808

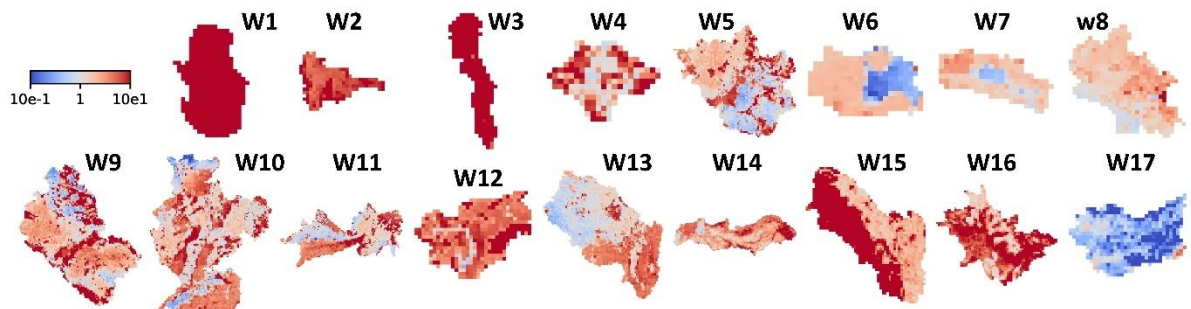
(a) Nitrogen inputs [kg/ha yr]



(b) Soil denitrification [kg/ha yr]



(c) Damköhler number [-]



809

810 Figure 107. The simulated long-term average (1982-2024) of nitrogen inputs, soil denitrification, and
811 Damköhler number.

812

813

814 **Tables**

815 Table 1. Characteristics of the selected catchments. **Lat** depicts the latitude of upper left corner of the
 816 catchment. **DEM** and **Area** are the mean elevation in m.a.s.l. and catchment size in km². **Precip**, **Temp**,
 817 and **PET** are the annual averages of precipitation, air temperature, and potential evapotranspiration
 818 in mm/yr. f_{crop} , f_{forest} , and f_{urban} are the fractions of cropland, forest, and urbanized areas in 2019
 819 in %. Null means no name is assigned for the catchment in the Catchment Characterisation and
 820 Modelling (CCM) database.

ID	Name	Lat	Area	DEM	Precip	Temp	PET	f_{crop}	f_{forest}	f_{urban}
1	Null	70.0	8725	468.5	448.5	-1.8	442.8	<1	1.9	<1
2	Vefsna	65.9	5475	636.5	1260.8	0.7	433.6	<1	24.6	<1
3	Null	59.8	5225	742.3	1400.9	3.0	545.7	<1	39.8	<1
4	Null	58.3	4350	67.4	654.5	6.4	667.9	17.4	60.5	1.4
5	Nemunas	56.6	97550	147.9	599.3	7.1	730.6	33.0	39.1	4.5
6	Tweed	55.9	6250	264.3	1023.4	7.9	600.9	21.8	18.9	1.4
7	Null	52.3	4300	175.4	1218.1	10.1	645.2	12.1	17.4	1.9
8	Thames	52.2	11900	112.0	700.7	10.4	782.9	44.9	14.1	22.0
9	Elbe	53.5	130225	318.3	626.9	8.8	836.3	41.2	34.6	10.8
10	Rhine	52.0	170175	508.3	943.3	8.9	821.0	21.5	41.2	17.1
11	Danube _(a)	50.5	197600	618.0	843.6	8.3	857.4	28.5	37.1	11.5
12	Adige	47.2	11600	1771.9	1002.3	4.5	809.7	<1	48.8	3.2
13	Loire	48.7	122125	298.9	778.7	11.0	887.4	37.6	25.7	6.5
14	Tajo	40.4	75575	686.2	549.5	14.3	1359.6	26.7	34.5	3.3
15	Danube _(b)	48.4	37975	533.3	534.7	8.1	869.5	32.0	41.3	6.4
16	Danube _(c)	44.8	37725	653.3	684.7	9.7	994.2	12.8	44.3	5.8
17	Null	37.6	12650	1384.5	454.1	12.2	1256.9	5.9	4.3	<1

821

822

823 Table 2. The calibration performance of discharge (Q), in-stream isotopes (¹⁸O, Iso), and nitrate (NO³⁻
824 N). Evaluation metrics include Kling-Gupta efficiency (~~KGE~~, →, (-)), Root Mean Square Error (~~RMSE~~;
825 m³/s, ‰, and mg/L for discharge, isotopes, and nitrate, respectively), Pearson Correlation Coefficient
826 (~~Coefficient~~; →, (-)), and Percent bias (~~Pbias~~; %), (-).

Metric	Unit	Min	Max	Mean	Median
KGE Kling-Gupta efficiency (Q)	-	0.14	0.89	0.65	0.69
KGE Kling-Gupta efficiency (Iso)	-	-0.03	0.86	0.45	0.48
KGE Kling-Gupta efficiency (NO ³ -N)	-	-0.36	0.72	0.42	0.44
Correlation —(Q) Pearson correlation coefficient (Q)	-	0.49	0.92	0.79	0.81
Correlation Pearson correlation coefficient (Iso)	-	0.14	0.87	0.51	0.54
Correlation Pearson correlation coefficient (NO ³ -N)	-	-0.26	0.86	0.55	0.6
RMSE Root Mean Square Error (Q)	m ³ /s	3.99	677.08	123.02	68.51
RMSE Root Mean Square Error (Iso)	‰	0.31	1.51	0.72	0.73
RMSE Root Mean Square Error (NO ³ -N)	mg/L	0.02	2.82	0.83	0.57
Pbias Percent bias (Q)	%	0.52	79.88	17.44	9.53
Pbias Percent bias (Iso)	%	-11.28	-0.07	-4.3	-4.42
Pbias Percent bias (NO ³ -N)	%	0.18	49.25	15.52	10.89

827

828

829 **Reference**

- 830 Akbarzadeh, Z., Maavara, T., Slowinski, S., & Van Cappellen, P. (2019). Effects of Damming on River
831 Nitrogen Fluxes: A Global Analysis. *Global Biogeochemical Cycles*, 33.
832 <https://doi.org/10.1029/2019GB006222>
- 833 Ala-aho, P., Tetzlaff, D., Mcnamara, J., Laudon, H., & Kormos, P. (2017). Modeling the isotopic
834 evolution of snowpack and snowmelt: Testing a spatially distributed parsimonious approach.
835 *Water Resources Research*, 53. <https://doi.org/10.1002/2017WR020650>
- 836 Amato, M. T., & Giménez, D. (2024). Predicting monthly near-surface soil temperature from air
837 temperature and the leaf area index. *Agricultural and Forest Meteorology*, 345, 109838.
838 <https://doi.org/10.1016/j.agrformet.2023.109838>
- 839 Arnold, J., Moriasi, D., Gassman, P., Abbaspour, K., White, M., Srinivasan, R., et al. (2012). SWAT:
840 Model use, calibration, and validation. *Transactions of the ASABE (American Society of*
841 *Agricultural and Biological Engineers)*, 55. <https://doi.org/10.13031/2013.42256>
- 842 Bajracharya, A., Moghairib, M., Stadyk, T., & Asadzadeh, M. (2023). Process based calibration of a
843 continental-scale hydrological model using soil moisture and streamflow data. *Journal of*
844 *Hydrology: Regional Studies*, 47, 101391. <https://doi.org/10.1016/j.ejrh.2023.101391>
- 845 Benettin, P., Bailey, S., Campbell, J., Green, M., Rinaldo, A., Likens, G., et al. (2015). Linking water age
846 and solute dynamics in streamflow at the Hubbard Brook Experimental Forest, NH, USA.
847 *Water Resources Research*, 51, 9256–9272. <https://doi.org/10.1002/2015WR017552>
- 848 Beven, K. (2006). A manifesto for the equifinality thesis. *Journal of Hydrology*, 320(1–2), 18–36.
849 <https://doi.org/10.1016/J.JHYDROL.2005.07.007>
- 850 Beven, K. (2015). Facets of uncertainty: Epistemic uncertainty, non-stationarity, likelihood, hypothesis
851 testing, and communication. *Hydrological Sciences Journal*, 61, 150407155940006.
852 <https://doi.org/10.1080/02626667.2015.1031761>
- 853 Birkel, C., & Soulsby, C. (2015). Advancing tracer-aided rainfall-runoff modelling: A review of progress,
854 problems and unrealised potential. *Hydrological Processes*, 29(25), 5227–5240.
855 <https://doi.org/10.1002/HYP.10594>
- 856 Birkel, C., Tetzlaff, D., & Dunn, S. (2011). Using time domain and geographic source tracers to
857 conceptualize streamflow generation processes in lumped rainfall-runoff models. *Water*
858 *Resources Research - WATER RESOUR RES*, 47. <https://doi.org/10.1029/2010WR009547>
- 859 Bonchkovskiy, A., & Osadcha, N. (2024). Modelling of the nutrient load in the Sula River basin using
860 the MONERIS. *Physical Geography and Geomorphology*, 47, 7–20.
861 <https://doi.org/10.17721/phgg.2024.3-4.01>
- 862 Condon, L., Kollet, S., Bierkens, M., Maxwell, R., Hill, M., Franssen, H.-J., et al. (2021). Global
863 Groundwater Modeling and Monitoring: Opportunities and Challenges. *Water Resources*
864 *Research*, 57. <https://doi.org/10.1029/2020WR029500>
- 865 Craig, H., Gordon, L. I., & Horibe, Y. (1964). Isotopic exchange effects in the evaporation of water: 1.
866 Low-temperature experimental results. *Journal of Geophysical Research*, 68(17), 5079–5087.
867 <https://doi.org/10.1029/JZ068I017P05079>
- 868 Dawson, T., & Ehleringer, J. (1991). Streamside trees that do not use stream water. *Nature*, 350, 335–
869 337. <https://doi.org/10.1038/350335a0>
- 870 Dick, J. J., Tetzlaff, D., Birkel, C., & Soulsby, C. (2015). Modelling landscape controls on dissolved
871 organic carbon sources and fluxes to streams. *Biogeochemistry*, 122(2–3), 361–374.
872 <https://doi.org/10.1007/S10533-014-0046-3>
- 873 Donnelly, C., Andersson, J. C. M., & Arheimer, B. (2016). Using flow signatures and catchment
874 similarities to evaluate the E-HYPE multi-basin model across Europe. *Hydrological Sciences*
875 *Journal*, 61(2), 255–273. <https://doi.org/10.1080/02626667.2015.1027710>

876 Eckersten, H., Jansson, P. E., & Johnsson, H. (1994). SOILN model – user’s manual 2nd edition, Division
877 of Agricultural Hydrotechnics Communications, 94:4. Department of Soil Sciences, Swedish
878 University of Agricultural Sciences, 58pp, Uppsala.

879 Efstratiadis, A., & Koutsoyiannis, D. (2010). One decade of multi-objective calibration approaches in
880 hydrological modelling: A review. *Hydrological Sciences Journal*, 55(1), 58–78.
881 <https://doi.org/10.1080/02626660903526292>

882 Godsey, S. E., Aas, W., Clair, T. A., de Wit, H. A., Fernandez, I. J., Kahl, J. S., et al. (2010). Generality of
883 fractal 1/f scaling in catchment tracer time series, and its implications for catchment travel
884 time distributions. *Hydrological Processes*, 24(12), 1660–1671.
885 <https://doi.org/10.1002/hyp.7677>

886 Good, S. P., Soderberg, K., Guan, K., King, E. G., Scanlon, T. M., & Caylor, K. K. (2014). $\delta^2\text{H}$ isotopic flux
887 partitioning of evapotranspiration over a grass field following a water pulse and subsequent
888 dry down. *Water Resources Research*, 50(2), 1410–1432.
889 <https://doi.org/10.1002/2013WR014333>

890 Grizzetti, B., Vigiak, O., Udias, A., Aloe, A., Zanni, M., Bouraoui, F., et al. (2021). How EU policies could
891 reduce nutrient pollution in European inland and coastal waters. *Global Environmental*
892 *Change*, 69, 102281. <https://doi.org/10.1016/j.gloenvcha.2021.102281>

893 [Hersbach, H., Bell, B., Berrisford, P., Hirahara, S., Horányi, A., Muñoz Sabater, J., et al. \(2020\). The ERA5
894 global reanalysis. *Quarterly Journal of the Royal Meteorological Society*, 146.
895 <https://doi.org/10.1002/qj.3803>](https://doi.org/10.1002/qj.3803)

896 Hooper, R., Stone, A., Christophersen, N., de Melo, E., & Seip, H. (1988). Assessing the Birkenes Model
897 of Stream Acidification using a multi-signal calibration methodology. *Water Resources*
898 *Research - WATER RESOUR RES*, 24, 1308–1316. <https://doi.org/10.1029/WR024i008p01308>

899 Horita, J., Rozanski, K., & Cohen, S. (2008). Isotope effects in the evaporation of water: A status report
900 of the Craig-Gordon model. *Isotopes in Environmental and Health Studies*, 44, 23–49.
901 <https://doi.org/10.1080/10256010801887174>

902 Hrachowitz, M., Savenije, H., Bogaard, T. A., Tetzlaff, D., & Soulsby, C. (2013). What can flux tracking
903 teach us about water age distribution patterns and their temporal dynamics? *Hydrology and*
904 *Earth System Sciences*, 117(2), 533–564. <https://doi.org/10.5194/HESS-17-533-2013>

905 Huijgevoort, M., Tetzlaff, D., & Sutanudjaja, E. (2016). Using high resolution tracer data to constrain
906 water storage, flux and age estimates in a spatially distributed rainfall-runoff model.
907 *Hydrological Processes*, 30. <https://doi.org/10.1002/hyp.10902>

908 Jasechko, S., Kirchner, J., Welker, J., & McDonnell, J. (2016). Substantial proportion of global
909 streamflow less than three months old. *Nature Geoscience*, 9.
910 <https://doi.org/10.1038/NCEO2636>

911 Jones, E. R., Bierkens, M. F. P., Wanders, N., Sutanudjaja, E. H., van Beek, L. P. H., & van Vliet, M. T. H.
912 (2023). DynQual v1.0: a high-resolution global surface water quality model. *Geoscientific*
913 *Model Development*, 16(15), 4481–4500. <https://doi.org/10.5194/gmd-16-4481-2023>

914 Jung, H., Tetzlaff, D., Birkel, C., & Soulsby, C. (2025). Recent Developments and Emerging Challenges
915 in Tracer-Aided Modeling. *Wiley Interdisciplinary Reviews Water*, 12.
916 <https://doi.org/10.1002/wat2.70015>

917 Kale, R., & Sahoo, B. (2011). Green-Ampt Infiltration Models for Varied Field Conditions: A Revisit.
918 *Water Resources Management*, 25, 3505–3536. <https://doi.org/10.1007/s11269-011-9868-0>

919 Kumar, R., Samaniego, L., & Attinger, S. (2013). Implications of distributed hydrologic model
920 parameterization on water fluxes at multiple scales and locations. *Water Resources Research*,
921 49(1), 360–379. <https://doi.org/10.1029/2012WR012195>

- 922 Kuppel, S., Tetzlaff, D., Maneta, M., & Soulsby, C. (2018). EcH2O-iso 1.0: Water isotopes and age
 923 tracking in a process-based, distributed ecohydrological model. *Geoscientific Model*
 924 *Development*, 11, 3045–3069. <https://doi.org/10.5194/gmd-11-3045-2018>
- 925 Landgraf, J., Tetzlaff, D., Birkel, C., Stevenson, J., & Soulsby, C. (2023). Assessing land use effects on
 926 ecohydrological partitioning in the critical zone through isotope-aided modelling. *Earth*
 927 *Surface Processes and Landforms*, 48. <https://doi.org/10.1002/esp.5691>
- 928 Lindström, G., Pers, C., Rosberg, J., Strömqvist, J., & Arheimer, B. (2010). Development and test of the
 929 HYPE (Hydrological Predictions for the Environment) model – A water quality model for
 930 different spatial scales. *Hydrology Research*, 41. <https://doi.org/10.2166/nh.2010.007>
- 931 Maneta, M. P., & Silverman, N. L. (2013). A spatially distributed model to simulate water, energy, and
 932 vegetation dynamics using information from regional climate models. *Earth Interactions*,
 933 17(11), 1–44. <https://doi.org/10.1175/2012EI000472.1>
- 934 McDonnell, J. (2014). The two water worlds hypothesis: Ecohydrological separation of water between
 935 streams and trees? *Wiley Interdisciplinary Reviews: Water*, 1.
 936 <https://doi.org/10.1002/wat2.1027>
- 937 McDonnell, J., & Beven, K. (2014). Debates on Water Resources: The future of hydrological sciences:
 938 A (common) path forward? A call to action aimed at understanding velocities, celerities and
 939 residence time distributions of the headwater hydrograph. *Water Resources Research*, 50.
 940 <https://doi.org/10.1002/2013WR015141>
- 941 Mcmillan, H., Araki, R., Bolotin, L., Kim, D.-H., Coxon, G., Clark, M., & Seibert, J. (2025). Global patterns
 942 in observed hydrologic processes. *Nature Water*, 3. <https://doi.org/10.1038/s44221-025-00407-w>
- 944 Mikayilov, F., Rouholahnejad Freund, E., Ashraf Vaghefi, S., Srinivasan, R., Yang, H., & Klöve, B. (2015).
 945 A continental-scale hydrology and water quality model for Europe: Calibration and uncertainty
 946 of a high-resolution large-scale SWAT model. *Journal of Hydrology*, 524.
 947 <https://doi.org/10.1016/j.jhydrol.2015.03.027>
- 948 [Mu, Q., Zhao, M., & Running, S. \(2011\). Improvements to a MODIS Global Terrestrial](https://doi.org/10.1016/j.rse.2011.02.019)
 949 [Evapotranspiration Algorithm. *Remote Sensing of Environment*, 115, 1781–1800.](https://doi.org/10.1016/j.rse.2011.02.019)
 950 <https://doi.org/10.1016/j.rse.2011.02.019>
- 951 Nan, Y., He, Z., Tian, F., Wei, Z., & Tian, L. (2021). Can we use precipitation isotope outputs of isotopic
 952 general circulation models to improve hydrological modeling in large mountainous
 953 catchments on the Tibetan Plateau? *Hydrology and Earth System Sciences*, 25(12), 6151–6172.
 954 <https://doi.org/10.5194/hess-25-6151-2021>
- 955 Naz, B. S., Sharples, W., Ma, Y., Goergen, K., & Kollet, S. (2023). Continental-scale evaluation of a fully
 956 distributed coupled land surface and groundwater model, ParFlow-CLM (v3.6.0), over Europe.
 957 *Geoscientific Model Development*, 16(6), 1617–1639. <https://doi.org/10.5194/gmd-16-1617-2023>
- 959 Neal, C., Christophersen, N., Neale, R., Smith, C., & Reynolds, B. (1988). Chloride in precipitation and
 960 streamwater for the upland catchment of River Severn, mid- Wales; some consequences for
 961 hydrochemical models. *Hydrological Processes*, 2, 155–165.
 962 <https://doi.org/10.1002/hyp.3360020206>
- 963 Nearing, G., Ruddell, B., Bennett, A., Prieto, C., & Gupta, H. (2020). Does Information Theory Provide
 964 a New Paradigm for Earth Science? Hypothesis Testing. *Water Resources Research*, 56.
 965 <https://doi.org/10.1029/2019WR024918>
- 966 Ocampo, C., Sivapalan, M., & Oldham, C. (2006). Hydrological connectivity of upland-riparian zones in
 967 agricultural catchments: Implications for runoff generation and nitrate transport. *Journal of*
 968 *Hydrology*, 331, 643–658. <https://doi.org/10.1016/j.jhydrol.2006.06.010>

- 969 Pechlivanidis, I., Jackson, B., McIntyre, N., & Wheeler, H. (2011). Catchment scale hydrological
970 modelling: A review of model types, calibration approaches and uncertainty analysis methods
971 in the context of recent developments in technology and applications. *GlobalNEST*
972 *International Journal*, 13, 193–214.
- 973 Pesántez, J., Birkel, C., Gaona, G., Arciniega-Esparza, S., Murray, D., Mosquera, G., et al. (2023).
974 Spatially distributed tracer-aided modelling to explore DOC dynamics, hot spots and hot
975 moments in a tropical mountain catchment. *Hydrological Processes*, 37, 1–15.
976 <https://doi.org/10.1002/hyp.15020>
- 977 Rakovec, O., Kumar, R., Mai, J., Cuntz, M., Thober, S., Zink, M., et al. (2016). Multiscale and Multivariate
978 Evaluation of Water Fluxes and States over European River Basins. *Journal of*
979 *Hydrometeorology*, 17, 287–307. <https://doi.org/10.1175/JHM-D-15-0054.1>
- 980 Rakovec, O., Mizukami, N., Kumar, R., Newman, A., Thober, S., Wood, A., et al. (2019). Diagnostic
981 Evaluation of Large-Domain Hydrologic Models Calibrated Across the Contiguous United
982 States. *Journal of Geophysical Research: Atmospheres*, 124.
983 <https://doi.org/10.1029/2019JD030767>
- 984 Remondi, F., Kirchner, J., Burlando, P., & Fatichi, S. (2018). Water Flux Tracking with A Distributed
985 Hydrological Model to Quantify Controls on the Spatio-Temporal Variability of Transit Time
986 Distributions. *Water Resources Research*, 54. <https://doi.org/10.1002/2017WR021689>
- 987 Samaniego, L., Kumar, R., & Attinger, S. (2010). Multiscale parameter regionalization of a grid-based
988 hydrologic model at the mesoscale. *Water Resour. Res.*, 46.
989 <https://doi.org/10.1029/2008WR007327>
- 990 Seybold, E., Dwivedi, R., Musselman, K., Kincaid, D., Schroth, A., Classen, A., et al. (2022). Winter runoff
991 events pose an unquantified continental-scale risk of high wintertime nutrient export.
992 *Environmental Research Letters*, 17, 104044. <https://doi.org/10.1088/1748-9326/ac8be5>
- 993 Šimůnek, J., Šejna, M., Saito, H., & Van Genuchten, M. T. (2013). *The HYDRUS-1D software package*
994 *for simulating the one-dimensional movement of water, heat, and multiple solutes in variably-*
995 *saturated media (Version 4.17)*. Department of Environmental Sciences University of Riverside
996 California, California.
- 997 Skrzypek, G., Mydłowski, A., Dogramaci, S., Hedley, P., Gibson, J. J., & Grierson, P. F. (2015). Estimation
998 of evaporative loss based on the stable isotope composition of water using Hydrocalculator.
999 *Journal of Hydrology*, 523, 781–789. <https://doi.org/10.1016/j.jhydrol.2015.02.010>
- 1000 Smith, A., Tetzlaff, D., Kleine, L., Maneta, M., & Soulsby, C. (2021). Quantifying the effects of land use
1001 and model scale on water partitioning and water ages using tracer-aided ecohydrological
1002 models. *Hydrology and Earth System Sciences*, 25, 2239–2259. [https://doi.org/10.5194/hess-](https://doi.org/10.5194/hess-25-2239-2021)
1003 [25-2239-2021](https://doi.org/10.5194/hess-25-2239-2021)
- 1004 Soulsby, C., Birkel, C., Geris, J., Dick, J., Tunaley, C., & Tetzlaff, D. (2015). Stream water age distributions
1005 controlled by storage dynamics and nonlinear hydrologic connectivity: Modeling with high-
1006 resolution isotope data. *Water Resources Research*, 51(9), 7759–7776.
1007 <https://doi.org/10.1002/2015WR017888>
- 1008 Sprenger, M., Stumpp, C., Weiler, M., Aeschbach, W., Allen, S., Benettin, P., et al. (2019). The
1009 Demographics of Water: A Review of Water Ages in the Critical Zone. *Reviews of Geophysics*,
1010 57. <https://doi.org/10.1029/2018RG000633>
- 1011 [Tapley, B., Bettadpur, S., Ries, J. C., Thompson, P., & Watkins, M. \(2004\). GRACE Measurements of](https://doi.org/10.1126/science.1099192)
1012 [Mass Variability in the Earth System. *Science \(New York, N.Y.\)*, 305, 503–5.](https://doi.org/10.1126/science.1099192)
1013 <https://doi.org/10.1126/science.1099192>
- 1014 Tetzlaff, D., Buttle, J., Carey, S. K., Mcguire, K., Laudon, H., & Soulsby, C. (2015). Tracer-based
1015 assessment of flow paths, storage and runoff generation in northern catchments: A review.
1016 *Hydrological Processes*, 29(16), 3475–3490. <https://doi.org/10.1002/HYP.10412>

- 1017 Wang, J., Bouwman, A., Vilmin, L., Beusen, A., Hoek, W., Liu, X., & Middelburg, J. (2024). Global inland-
 1018 water nitrogen cycling has accelerated in the Anthropocene. *Nature Water*, 2.
 1019 <https://doi.org/10.1038/s44221-024-00282-x>
- 1020 Wellen, C., Kamran-Disfani, A.-R., & Arhonditsis, G. (2015). Evaluation of the Current State of
 1021 Distributed Watershed Nutrient Water Quality Modeling. *Environmental Science &*
 1022 *Technology*, 49. <https://doi.org/10.1021/es5049557>
- 1023 Wen, Y., Lin, J.-S., Plaza, F., & Liang, X. (2024). Roles of Hydrology and Transport Processes in
 1024 Denitrification at Watershed Scale. *Water Resources Research*, 60, 1–24.
 1025 <https://doi.org/10.1029/2023WR034971>
- 1026 Winkler, K., Fuchs, R., Rounsevell, M., & Herold, M. (2021). Global land use changes are four times
 1027 greater than previously estimated. *Nature Communications*, 12(1), 2501.
 1028 <https://doi.org/10.1038/s41467-021-22702-2>
- 1029 Wu, S., Tetzlaff, D., Yang, X., & Soulsby, C. (2022). Disentangling the influence of landscape
 1030 characteristics, hydroclimatic variability and land management on surface water NO₃-N
 1031 dynamics: spatially distributed modelling over 30 years in a lowland mixed land use catchment.
 1032 *Water Resources Research*, e2021WR030566. <https://doi.org/10.1029/2021WR030566>
- 1033 Wu, S., Tetzlaff, D., Beven, K., & Soulsby, C. (2025a). DREAM(LoAX): Simultaneous Calibration and
 1034 Diagnosis for Tracer-Aided Ecohydrological Models Under the Equifinality Thesis. *Water*
 1035 *Resources Research*, 61, e2024WR038779. <https://doi.org/10.1029/2024WR038779>
- 1036 Wu, S., Tetzlaff, D., Yang, X., Sauter, T., & Soulsby, C. (2025b). Hydrological Connectivity Dominates
 1037 NO₃-N Cycling in Complex Landscapes – Insights From Integration of Isotopes and Water
 1038 Quality Modeling. *Water Resources Research*, 61, e2025WR040525.
 1039 <https://doi.org/10.1029/2025WR040525>
- 1040 Wu, S., Tetzlaff, D., & Soulsby, C. (2025c). Revising Common Approaches for Calibration: Insights From
 1041 a 1-D Tracer-Aided Hydrological Model With High-Dimensional Parameters and Objectives.
 1042 *Water Resources Research*, 61, e2024WR037656. <https://doi.org/10.1029/2024WR037656>
- 1043 Wu, S., Tetzlaff, D., Zheng, Y., & Soulsby, C. (2025d). EcoTWIN v1.0 release.
 1044 <https://doi.org/10.5281/zenodo.16747633>
- 1045 Yang, C., Condon, L., & Maxwell, R. (2025). Unravelling groundwater–stream connections over the
 1046 continental United States. *Nature Water*, 3. <https://doi.org/10.1038/s44221-024-00366-8>
- 1047 Yang, X., Jomaa, S., Zink, M., Fleckenstein, J., Borchardt, D., & Rode, M. (2018). A New Fully Distributed
 1048 Model of Nitrate Transport and Removal at Catchment Scale. *Water Resources Research*, 54.
 1049 <https://doi.org/10.1029/2017WR022380>
- 1050 Yang, X., Zhang, X., Graeber, D., Hensley, R., Jarvie, H., Lorke, A., et al. (2023a). Large-stream nitrate
 1051 retention patterns shift during droughts: Seasonal to sub-daily insights from high-frequency
 1052 data-model fusion. *Water Research*, 243, 120347.
 1053 <https://doi.org/10.1016/j.watres.2023.120347>
- 1054 Yang, X., Tetzlaff, D., Müller, C., Knöller, K., Borchardt, D., & Soulsby, C. (2023b). Upscaling Tracer-
 1055 Aided Ecohydrological Modeling to Larger Catchments: Implications for Process
 1056 Representation and Heterogeneity in Landscape Organization. *Water Resources Research*, 59,
 1057 e2022WR033033. <https://doi.org/10.1029/2022WR033033>
- 1058 Yang, X., Tetzlaff, D., Jin, J., Li, Q., Borchardt, D., & Soulsby, C. (2024). Linking terrestrial biogeochemical
 1059 processes and water ages to catchment water quality: A new Damköhler analysis based on
 1060 coupled modeling of isotope tracers and nitrate dynamics. *Water Research*, 262, 122118.
 1061 <https://doi.org/10.1016/j.watres.2024.122118>
- 1062 Zhang, Z., Chen, X., Cheng, Q.-B., Li, S.-L., Yue, F.-J., Peng, T., et al. (2020). Coupled hydrological and
 1063 biogeochemical modelling of nitrogen transport in the karst critical zone. *Science of The Total*
 1064 *Environment*, 732, 138902. <https://doi.org/10.1016/j.scitotenv.2020.138902>

1065 Zhu, J., Jia, Y., Yu, G., Wang, Q., He, N., Chen, Z., et al. (2025). Changing patterns of global nitrogen
1066 deposition driven by socio-economic development. *Nature Communications*, 16(1), 46.
1067 <https://doi.org/10.1038/s41467-024-55606-y>
1068